Evaluation of Rho kinase inhibitor effects on neuroprotection and neuroinflammation in an ex-vivo retinal explant model

Élodie Reboussin, Paul Bastelica, Ilyes Benmessabih, Arnaud Cordovilla, Cécile Delarasse, Annabelle Réaux-Le Goazigo, Françoise Brignole-Baudouin, Céline Olmière, Christophe Baudouin, Juliette Buffault, et al.

Reboussin *et al.*
Acta Neuropathologica Communications (2024) 12:150
https://doi.org/10.1186/s40478-024-01859-z

Acta Neuropathologica Communications

RESEARCH

Open Access

Evaluation of Rho kinase inhibitor effects on neuroprotection and neuroinflammation in an ex-vivo retinal explant model

Élodie Reboussin[1], Paul Bastelica[1,3,4], Ilyes Benmessabih[1], Arnaud Cordovilla[1], Cécile Delarasse[1], Annabelle Réaux-Le Goazigo[1], Françoise Brignole-Baudouin[1,2,3,4], Céline Olmière[7], Christophe Baudouin[1,3,5,6†], Juliette Buffault[1,3,5,6†] and Stéphane Mélik Parsadaniantz[1*†]

Abstract

Background Glaucoma is a leading cause of blindness, affecting retinal ganglion cells (RGCs) and their axons. By 2040, it is likely to affect 110 million people. Neuroinflammation, specifically through the release of proinflammatory cytokines by M1 microglial cells, plays a crucial role in glaucoma progression. Indeed, in post-mortem human studies, pre-clinical models, and ex-vivo models, RGC degeneration has been consistently shown to be linked to inflammation in response to cell death and tissue damage. Recently, Rho kinase inhibitors (ROCKis) have emerged as potential therapies for neuroinflammatory and neurodegenerative diseases. This study aimed to investigate the potential effects of three ROCKis (Y-27632, Y-33075, and H-1152) on retinal ganglion cell (RGC) loss and retinal neuroinflammation using an ex-vivo retinal explant model.

Methods Rat retinal explants underwent optic nerve axotomy and were treated with Y-27632, Y-33075, or H-1152. The neuroprotective effects on RGCs were evaluated using immunofluorescence and Brn3a-specific markers. Reactive glia and microglial activation were studied by GFAP, CD68, and Iba1 staining. Flow cytometry was used to quantify day ex-vivo 4 (DEV 4) microglial proliferation and M1 activation by measuring the number of $CD11b^+$, $CD68^+$, and $CD11b^+/CD68^+$ cells after treatment with control solvent or Y-33075. The modulation of gene expression was measured by RNA-seq analysis on control and Y-33075-treated explants and glial and pro-inflammatory cytokine gene expression was validated by RT-qPCR.

Results Y-27632 and H-1152 did not significantly protect RGCs. By contrast, at DEV 4, 50 µM Y-33075 significantly increased RGC survival. Immunohistology showed a reduced number of $Iba1^+/CD68^+$ cells and limited astrogliosis with Y-33075 treatment. Flow cytometry confirmed lower $CD11b^+$, $CD68^+$, and $CD11b^+/CD68^+$ cell numbers in the Y-33075 group. RNA-seq showed Y-33075 inhibited the expression of M1 microglial markers (*Tnfa*, *Il-1β*, *Nos2*) and glial markers (*Gfap*, *Itgam*, *Cd68*) and to reduce apoptosis, ferroptosis, inflammasome formation, complement activation, TLR pathway activation, and *P2rx7* and *Gpr84* gene expression. Conversely, Y-33075 upregulated RGC-specific markers, neurofilament formation, and neurotransmitter regulator expression, consistent with its neuroprotective effects.

†Co-direction of the work: Christophe Baudouin, Juliette Buffault and Stéphane Mélik Parsadaniantz.

*Correspondence:
Stéphane Mélik Parsadaniantz
stephane.melik-parsadaniantz@inserm.fr
Full list of author information is available at the end of the article

Conclusion Y-33075 demonstrates marked neuroprotective and anti-inflammatory effects, surpassing the other tested ROCKis (Y-27632 and H-1152) in preventing RGC death and reducing microglial inflammatory responses. These findings highlight its potential as a therapeutic option for glaucoma.

Keywords Glaucoma, Rho kinase inhibitor, Neuroprotection, Immunomodulation, RNAseq analysis, Retinal explant

Background

Glaucoma is a sight-threatening optic neuropathy in which RGC death leads to blindness if left untreated. Ocular hypertension is a well-known risk factor that promotes glaucoma development [1]. Current therapeutic strategies manage intraocular pressure (IOP) through the topical administration of pressure-lowering agents, such as prostaglandin analogs and beta blockers, surgical procedures, such as filtering surgery, and laser procedures, such as trabeculoplasty [2, 3]. However, these strategies are insufficient to prevent glaucoma progression and only delay the loss of vision. Moreover, in normal-tension glaucoma, the benefit of managing IOP is not well established, and hypotensive strategies are inefficient [4]. Promoting RGC survival through neuroprotective strategies could dramatically modify the poor visual prognosis of patients with glaucoma. Neuroinflammation appears to be a major element in glaucoma progression [5, 6]. Early retinal reactivity of glial cells e.g., microglial cells, Müller cells, and astrocytes, has been observed in the central visual pathway of glaucoma patients. This inflammatory component of the pathology has also been observed in preclinical models of ocular hypertension [7, 8]. Thus, the control of inflammatory cells and immunomodulation could represent a powerful therapeutic approach [9–12]. Upon activation, these cells release a cocktail of cytokines, chemokines, and reactive oxygen species (ROS) that subsequently contribute to RGC loss [13, 14]. More precisely, during retinal degeneration, microglial cells become activated and specifically polarize to a pro-inflammatory phenotype (also called M1). The M1 microglial state is characterized by the secretion of various pro-inflammatory cytokines, such as TNFα, IL-1β, and IL-6, the expression of cell-surface markers such as CD68, and the production of ROS [15, 16]. Compounds able to protect RGCs or delay RGC death and reduce the pro-inflammatory M1 phenotype could constitute a promising therapeutic option [17, 18].

A new concept of treatment that acts directly on the trabecular cytoskeleton has recently emerged. Rho-kinase inhibitors (ROCKis) specifically target cellular pathways involved in the modification of the cytoskeleton and extracellular matrix and decrease IOP by increasing aqueous humor (HA) outflow [19, 20]. These inhibitors target the Rho family proteins, including Rho-A, B, C, and E, consisting of small G proteins that become activated after binding to guanosine triphosphate (GTP). These factors are mainly involved in various cellular functions, including proliferation, adhesion, morphology, motor function, apoptosis, and neurite elongation. Rho-kinases (ROCKs) are the downstream effectors of Rho proteins. ROCK1 and ROCK2, the two isoforms of these protein kinases, share 65% homology, of which 87% is in the kinase domain. Their level of expression varies depending on the tissue type, the ROCK2 isoform being the predominant isoform in the eye. ROCK1 and ROCK2 are activated by two pathways, the "Rho-A-dependent" pathway, in which ROCK activation is dependent on the binding of Rho-A-GTP to the Rho binding domain (RBD), and a second pathway that allows ROCK activation through caspase-3 or granzyme B [21, 22]. Such activation enables the unfolding of ROCK and its transition to the active form, with numerous targets, including substrates involved in cell adhesion, neurite retraction, phagocytosis, apoptosis, cell migration, etc. More recently, the potential roles of ROCKis in neuroprotection (maintenance of neuronal structure and function) and axonal regeneration have been investigated in neurological diseases, such as spinal cord injury, Alzheimer's disease, multiple sclerosis, and glaucoma [20, 23–27]. Some ROCKis have also demonstrated an anti-inflammatory role by acting on intracellular signaling pathways involved in inflammation, and by modulating the activation state of glial cells [28–30].

Numerous animal models have been developed, but they face challenges concerning the reproducibility of RGC loss rates. Unlike cell lines or dissociated RGC cultures, we have recently developed and utilized a neuroretinal explant model [32]. This model preserves the multicellular and layered architecture of the retina, closely mimicking in-vivo conditions, with natural intercellular interactions and cellular responses. It allows direct access to the RGC layer, reduces the number of animals used, and is less time-consuming than conventional animal models, given the degeneration rate of RGCs [33–35]. Optic nerve transection induces the death of 90% of injured RGCs within 14 days post axotomy [36]. Thus, this model is a useful intermediary model between in vivo models, which are pertinent but time/cost/animal-consuming, and rapid/high-throughput cell culture models, which are often based on a

single cell type and insufficiently relevant to reflect the complexity of an entire tissue.

This study aimed to explore the effects of three ROCKis (Y-27632, Y-33075, and H-1152) on RGC loss and retinal neuroinflammation. Using an ex-vivo adult rat retinal explant model that mimics key features of glaucoma, such as RGC degeneration and inflammation, we used immunohistology and transcriptomic RNA-seq analysis to assess these effects [37].

Materials and methods

Animals

Adult (8-week-old) male Long Evans rats weighing 250–300 g were purchased from Janvier Laboratories. Animals were kept in pathogen-free conditions with food and water ad libitum and housed in a 12-h light/12-h dark cycle. All experiments were conducted after evaluation and approval by the Institutional Animal Care and Use Committee following the guidelines of Directive 2010/63/EU of the European Parliament on the protection of animals used for scientific purposes.

Retinal explant cultures

Retinal explant culture was performed as previously described in Reboussin et al. [32]. Briefly, eight-week-old Long Evans rats were used to collect retinal explants for culture. Rats were euthanized, and the eyes were excised and quickly placed in an ice-cold CO_2 independent medium (Thermo Fisher Scientific, ref. 18,045-054). Under sterile conditions at 4 °C, the anterior chamber, lens, and vitreous body were removed, and the retina was separated from the surrounding ocular tissues by dissection with curved micro-forceps. Then, retinas were cut into four equal quarters and flat-mounted with the RGC layer facing up on Millicell-polytetrafluoroethylene (PTFE) 0.4-µm culture plate inserts (Merck Millipore, ref. PICM01250) in culture medium composed of Neurobasal A (Thermo Fisher Scientific, ref. 10,888,022), 2% B27 supplement (Thermo Fisher Scientific, ref. 0080085-SA), 1% N2 supplement (Thermo Fisher Scientific, ref. 17,502,048), L-glutamine (Thermo Fisher Scientific, ref. 25,030,032), and 1% penicillin-streptomycin 10,000 U/mL at 37 °C in a humidified 5% CO_2 environment. Half of the medium was refreshed after 24 h and then changed every 48 h thereafter.

Pharmacological agent screening

ROCKis Y-27632, Y-33075, and H-1152 were purchased from MedChemExpress (Monmouth Junction, NJ, USA). They were all dissolved in DPBS following the supplier recommendations to prepare stock solutions and then diluted daily in retinal culture medium to the final concentrations used in the experiments (Table 1). They were directly applied to the RGC in a 3-µl droplet carefully dispensed onto the surface of the explants daily and added to the culture medium.

Immunohistochemistry

Tissue preparation

For cryosections, retinal explants were fixed in 4% PFA for 1 h at 4 °C and then dehydrated in 30% sucrose (Dulbecco's phosphate buffer saline (DPBS); pH 7.4) overnight at 4 °C, before being embedded in OCT (Tissue-Tek® O.C.T. Compound, Sakura® Finetek) and frozen in liquid nitrogen. Twelve-micrometer thick cryosections of retinal explants were produced using a Leica CM 3050S cryostat and stored at − 20 °C until immunostaining. For wholemount counting, retinal explants were fixed in 4% PFA at 4 °C for 1 h and rinsed in DPBS before the immunofluorescence step.

Immunofluorescence labeling of whole flat-mounted retinal explants and cryosections

Retinal explant wholemounts or cryosections were incubated for 2 h at room temperature (RT) in a blocking buffer (5% bovine serum albumin (BSA), 2% Triton X-100, and 0.5% Tween 20, in DPBS) and incubated overnight at 4 °C in incubation buffer (2.5% BSA, 1% Triton X-100 and 0.25% Tween 20 in DPBS) with monoclonal mouse anti-Brn-3a (1/100, Merck Millipore, ref. MAB1585), monoclonal mouse anti-CD68 (1/400, AbD Serotec, ref. MCA341R), polyclonal rabbit anti-GFAP (1/500, Dako, Agilent, ref. Z033429-2), and polyclonal rabbit anti-Iba1 (1/500, Wako, ref. W1W019-19741). Explant wholemounts or cryosections were washed three times in DPBS and incubated with an Alexa Fluor 594-conjugated donkey anti-mouse immunoglobulin

Table 1 ROCKis provided by MedChemExpress, with the stock solution and working solution concentrations

Rock inhibitor	Supplier	Stock solution (mM)	Working solution (µM)
Y-27632 dihydrochloride	MedChemExpress #HY-10583	100	500
Y-33075 dihydrochloride	MedChemExpress #HY-10069	10	50
H-1152 dihydrochloride	MedChemExpress #HY-15720A	20	100

(1/500, Thermo Fisher Scientific, ref. A21203) or an Alexa Fluor 488-conjugated donkey anti-rabbit immunoglobulin (1/500, Thermo Fisher Scientific, ref. A21206) as secondary antibodies (Thermo Fisher Scientific). The nuclei were stained with DAPI (1/500) for 1 h, at RT. Finally, retinal explant wholemounts or cryosections were washed and mounted in Fluoromount (Sigma Aldrich, ref. F4680-25ML).

Histological analysis and immunostaining quantification

For RGC quantification in wholemount retinas, imaging was performed at 20 × magnification (665 μm^2) using an epifluorescence microscope (Zeiss AX-10). Retinal ganglion cells were identified based on the Brn3a-specific marker. Images were captured at four locations from the optic nerve to the peripheral retina for each explant. Cells were counted manually using image analysis software (ImageJ, the United States National Institutes of Health (NIH)) and the *cell counter plugin* and are expressed as the "number of $Brn3a^+$ RGCs/field". Images for GFAP, Iba1, and CD68 immunostaining of cryosections or wholemount explants were captured using an inverted confocal microscope (Olympus, FV1000) at × 20 or × 40 magnification.

Microglia identification and flow cytometry analysis

At day ex-vivo (DEV) 4, retinal explants from the control solvent and Y-33075 groups were collected (n = 7–17) and dissociated using Liberase TL (Roche, ref. 05401020001) in DPBS for 30 min at 37 °C. Retinal explants were then dissociated and suspended by pipetting, filtered through a 70-µM filter, and centrifuged at 500×*g* for 5 min at 4 °C. Retinal cell pellets were then incubated with ViobilityTM fixable dye 405/520 (1/100, Miltenyi Biotec, ref. 130-130-421) and then anti-CD11b-PE (1/100, Biorad, MCA275PE) and anti-CD68-Alexa 647 (1/100, Biorad, MCA341A647) antibodies. We selected CD11b, a widely used microglial marker that identifies both non-activated and activated phenotypes, as the membrane antigen marker for FACS analysis. CD68 was chosen as a marker specifically expressed in activated microglia. Using the ratio of these markers allows us to account for variability in microglial cell numbers, whether activated or not, which can vary due to differences in explant size. To quantify the degree of inflammation accurately, it is necessary to use this ratio. Flow cytometry was performed on a FACS Celesta SORP (BD Biosciences) and the results analyzed using FlowJo software (FlowJo, LLC).

Quantitative RT-PCR

Total RNA of retinal explants (3 mg/explant) was purified using the NucleoSpin RNA kit (Macherey–Nagel, ref. 740,955.250) according to the manufacturer's protocol. Total RNA was reverse-transcribed into cDNA using a High-Capacity RNA to cDNA kit (Life Technologies, ref. 4,368,814) according to the manufacturer's instructions. Real-time PCR was performed using the TaqMan Fast Advanced Master Mix (Applied Biosystems, ref. 4,444,963) and an Applied Biosystem Quant Studio 5 instrument (Applied Biosystems). The delta-delta Ct method (ddCt) was used to analyze relative gene expression. *Rps18* was used as a housekeeping gene.

RNA extraction and RNA-seq libraries

For whole transcriptome analysis, total RNA was extracted from retinal explants treated with 50 µM Y-00375 (n = 4) or control solvent (n = 4) and those left untreated on day 0 (DEV 0 group, n = 6) after tissue lysis using the NucleoSpin RNA kit (Macherey–Nagel, ref. 740,955.250) according to the manufacturer's protocol. Total RNA was quantified and its quality was determined using a BioAnalyser 2100 with the RNA 6000 Nano Kit (Agilent Technologies, Leuven, Belgium). RNA samples with a RIN > 7.3 were selected for RNA-seq analysis. mRNA libraries were prepared following the manufacturer's recommendations (mRNA stranded with ligation from ILLUMINA).

The final library preparation of pooled samples was sequenced on a Nextseq 2000 ILLUMINA device with a P2-200 cycle cartridge (2 × 400 million 100-base reads) corresponding to 2 × 28 million reads per sample after demultiplexing.

RNA-Seq data analysis and bioinformatic analysis of biological processes and pathways

Fastq files obtained from the sequencing were aligned using STAR (v2.7.9a) against the Rat reference genome from Ensembl v110 (generated 2023/08/29), with the option "quantMode GeneCounts" to extract the raw counts for each gene, and all count files were concatenated into a single file. A sample file was created with the sample data, including the conditions (control solvent, DEV 0, Y-33075 50 µM) and number of replicates. The count file and sample file were loaded into our in-house R Shiny application EYE DV seq (Plateforme Phénotypage Cellulaire et Tissulaire, Institut de la Vision, Paris, France). We added 1 to all counts in the count file to avoid any 0-read count errors. We then removed the genes with a total count of < 10 for all samples. Finally, DESeq2 (v1.40.2) analysis was performed comparing the groups defined in the 'condition' column, with 'control solvent' as the control group and 'Y-33075 50 µM' as the treated group. The results were then filtered for significant genes using the *p*-values (< 0.05, base mean minimum 500, exclusion of $\log_2$ fold change between − 2 and + 2), allowing us to obtain a total of 131 differentially

expressed genes. An enrichment analysis was performed to determine the involved pathways using the GO database (using the Bioconductor packages 'org.Rn.eg.db' (v 3.17.0) and 'clusterProfiler' (v 4.8.1)).

Statistical analysis

Statistical analyses were performed using GraphPad Prism 9. Data are presented as the mean ± SEM. Unpaired t-tests or Mann–Whitney tests were performed for unpaired comparisons of RGC viability after counting based on Brn3a staining, RNA-seq and RT-qPCR data analysis, and flow cytometry analysis.

Results

RGC degeneration and microglial response in a retinal explant culture model

As we previously reported [32], the best therapeutic window to assess neuroprotection by ROCKis and their effects on microglial cells was determined by evaluating RGC degeneration and microglial cell proliferation and activation following optic nerve axotomy in the retinal explant culture model. Thus, the Brn3a-specific RGC marker was used for RGC counting on DEV 0 and DEV 4 (Fig. 1a). Brn3a$^+$ RGC loss was significant on DEV 4 relative to DEV 0 (686 ± 13.45 vs. 381.9 ± 42.30 RGCs, $P = 0.0019$) (Fig. 1b). We then analyzed Iba1$^+$ and CD68$^+$ cells in wholemount retinal explants at DEV 0 and DEV 4 by immunostaining. We observed an increase in Iba1$^+$ and CD68$^+$ cell number showing morphological activation, such as a phenotype characterized by enlarged soma and ramifications and shortened processes (Fig. 1c). Assessment at DEV 4 allowed us to evaluate Y-27632, Y-33075, and H-1152 for their ability to prevent or delay RGC degeneration and control or prevent microglial cell activation and proliferation following optic nerve axotomy.

Y-33075 is neuroprotective for RGCs

To evaluate the capacity of each ROCKi to prevent RGC degeneration, we counted Brn3a$^+$ RGCs per field after exposing retinal explants to Y-27632, Y-33075, or H-1152 for four days. Exposure to 50 µM Y-33075 significantly improved Brn3a$^+$ RGC survival on DEV 4 relative to the control group (592.5 ± 23.86 vs. 392.4 ± 22.23 RGCs/field, $P < 0.0001$). Furthermore, there was no significant difference in Brn3a$^+$ RGC counts between the 50 µM Y-33075 group at DEV 4 and the initial count at DEV 0 (Fig. 2b), demonstrating the ability of Y-33075 to prevent or delay RGC death. By contrast, Y-27632 and H-1152 did not provide any neuroprotective effect on RGC survival at concentrations of 500 µM and 100 µM, respectively. Therefore, Y-33075 is the most effective ROCKi in delaying or preventing RGC death after four days of culture.

Y-33075, Y-27632, and H-1152 strongly decrease microglial cell proliferation and activated-like phenotype in wholemounts and retinal explants cryosections at DEV 4

We analyzed Iba1$^+$ and CD68$^+$ cells by immunostaining in wholemount retinal explants and retinal explant cryosections at DEV 0 and DEV 4 to determine the microglial response and their polarization phenotype following exposure to each ROCKi. Wholemount retinal explants were stained for Iba1 and imaged by confocal microscopy to determine the phenotype-like morphology of Iba1$^+$ cells. At DEV 0, microglial cells showed a resting-like morphology, with small cell bodies and thin ramifications. After four days in culture, the phenotype tended to show a reactive and activated form, with increased soma size and thicker ramifications and shortened processes (Fig. 3a). At DEV 0, Iba1$^+$ microglial cells were mostly located in the inner plexiform layer (INL) and ganglion cell layer (GCL), and no CD68$^+$ cells were found (Fig. 3b). The number of Iba1$^+$ and CD68$^+$ cells was higher in the control solvent group at DEV 4 than at DEV 0, with a morphological activation-like phenotype. The number of Iba1$^+$/CD68$^+$ cells was higher in the inner layers of the retina, comprising RGCs, the inner plexiform layer (IPL), inner nuclear layer (INL), and outer plexiform layer (OPL). However, exposure of retinal explants to ROCKis led to a lower number of Iba1$^+$ and CD68$^+$ cells in all retinal layers at DEV 4 than those exposed to the control solvent at DEV 4. The decrease was the greatest in the Y-33075 treated group for both Iba1 and CD68 immunostaining. FACS analysis to compare the Y-33075 and control solvent groups at DEV 4 definitively showed a significantly smaller microglial cell population in the Y-33075-treated group. This was shown by a clear decrease in the percentage of CD11b$^+$ (****$p < 0.0001$), CD68$^+$ ($p = 0.028$), and CD11b$^+$/CD68$^+$ ($p = 0.013$) cells (Fig. 3c). These data demonstrate that ROCKi exposure conferred limited microglial proliferation and activation in retinal explants at DEV 4 relative to the control solvent group. This limited microglial activation was confirmed by a resting morphology. Moreover, the distribution and activation of the microglial cells differed throughout the retina at DEV 4 between the ROCKi-treated and control solvent groups.

Y-33075 and H-1152 significantly limit astrogliosis to inner retinal explant layers in retinal explant cryosections at DEV 4

We performed GFAP immunostaining of retinal explant cryosections on DEV 0 and DEV 4 to evaluate astrogliosis induced by the culture conditions and ROCKi exposure (Fig. 4a). On DEV 0, GFAP immunoreactivity in astrocytes and Müller cells was mainly located in the nerve fiber layer (NFL) and OPL. However,

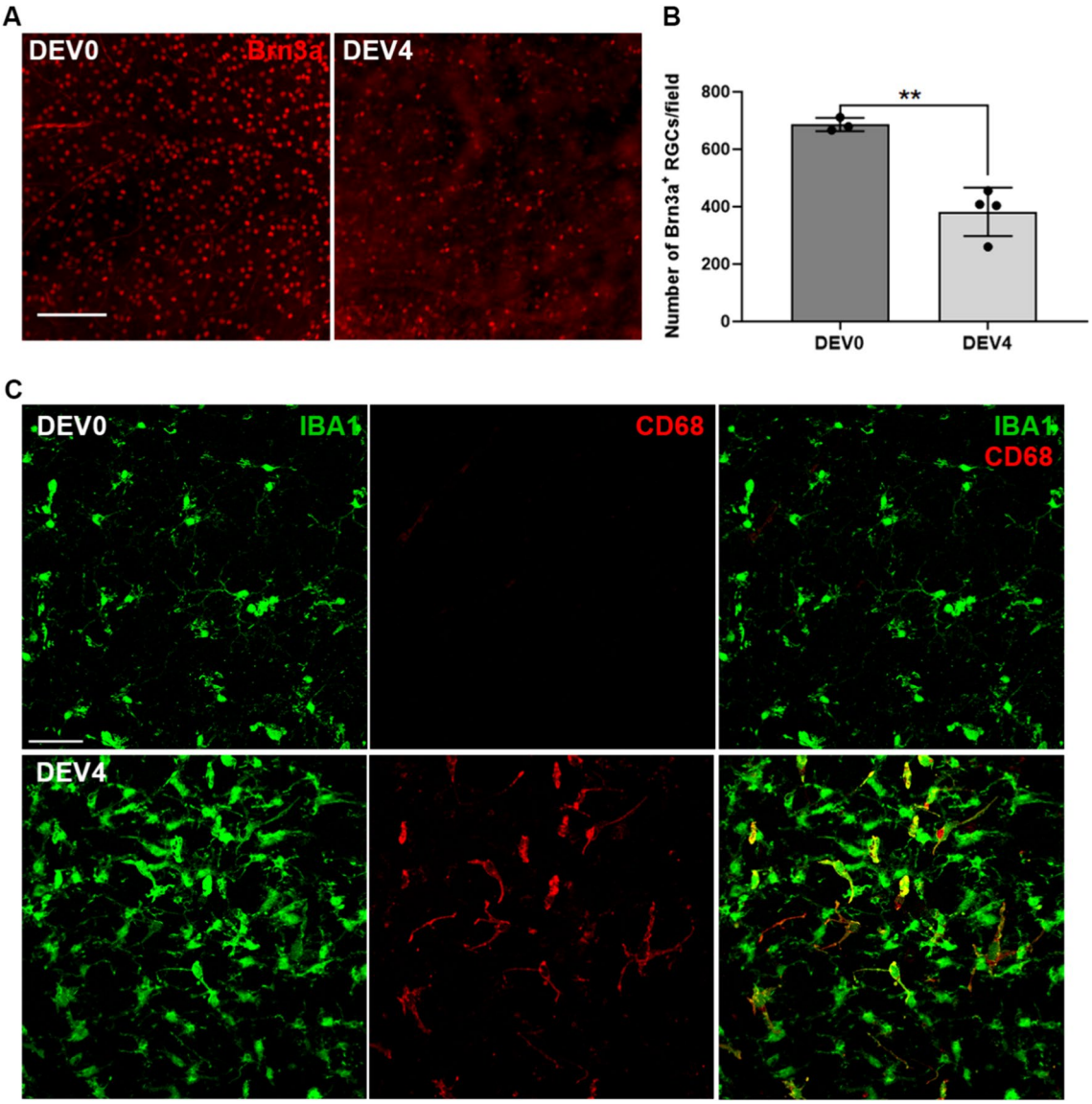

Fig. 1 RGC degeneration and microglial cell activation in neuroretinal explant culture. Representative images of wholemount retinal explants in culture from DEV 0 and DEV 4 immunolabeled with Brn3a at 20 × magnification (scale bar = 150 µm) (**a**) and quantification of Brn3a$^+$ RGCs (n = 3–4 per group) from wholemount retinal explants (**b**). Error bars indicate the standard error of the mean. $^{**}P = 0.0019$. (**c**) Representative confocal images of wholemount retinal explants in culture at DEV 0 (n = 4) and DEV 4 (n = 4) immunolabeled with Iba1 (green), and CD68 (red) at 40 × magnification (scale bar = 50 µm)

by DEV 4, GFAP immunoreactivity spread and was upregulated in all retinal layers in the control solvent and Y-27632 exposed groups, with the end-feet reaching the OPL and longer processes than on DEV 0. By contrast, GFAP immunostaining was limited to the NFL and, to a lesser extent, the OPL in the Y-33075- and H-1152-treated groups. To strengthen our results, we conducted RT-qPCR analysis of Gfap gene expression (Fig. 4b). Our findings confirmed the occurrence of astrogliosis between DEV 0 and DEV 4 in the control solvent group, as evidenced by a significant increase in Gfap gene expression ($^{***}p < 0.01$). Additionally, we observed that Gfap mRNA expression is significantly downregulated in the H-1152 treated group compared to the DEV 4 control solvent group. These data demonstrate that exposure to Y-33075 and H-1152 resulted in limited glial activation in retinal explants at DEV 4 relative to the control group.

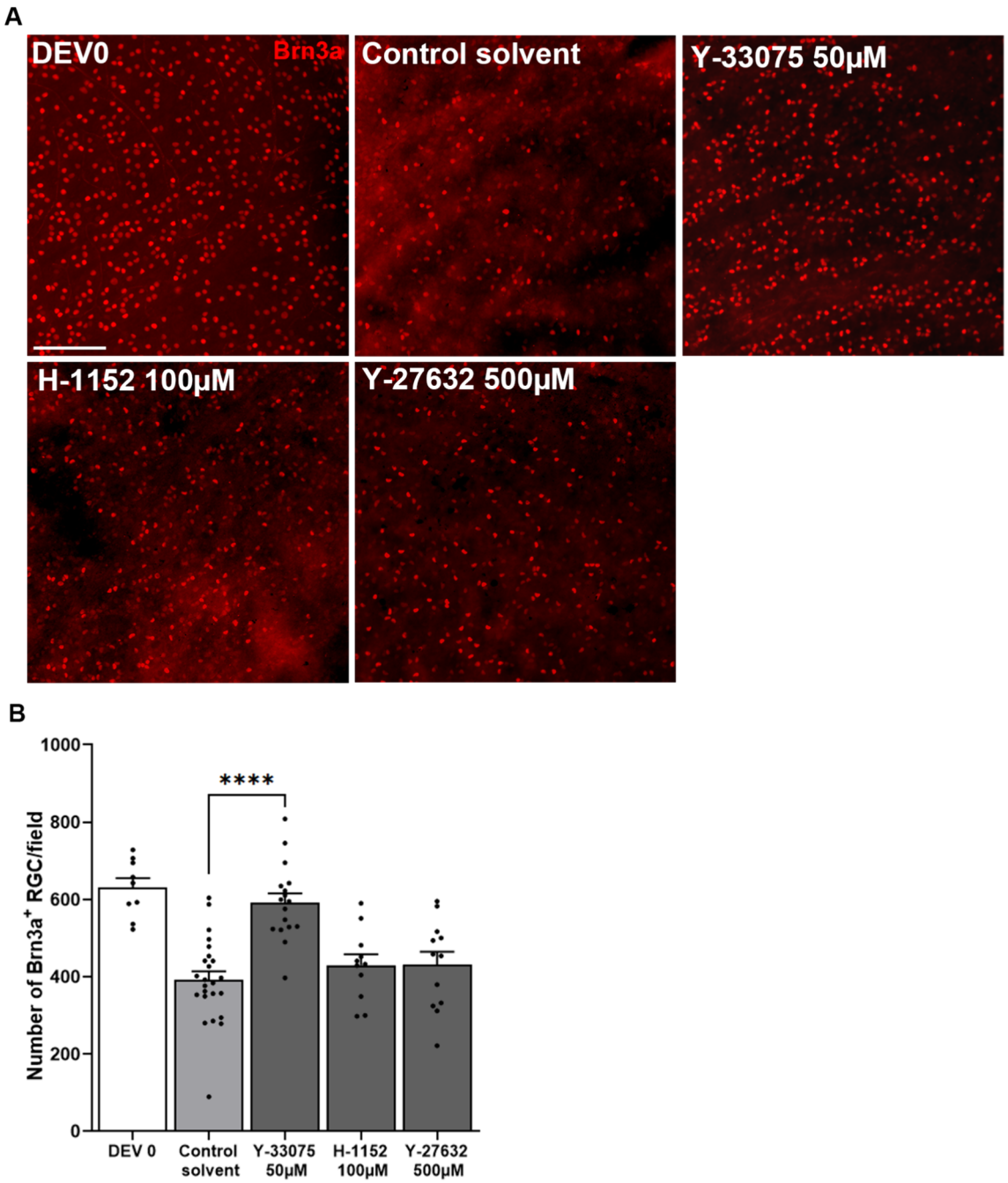

Fig. 2 Immunostaining of wholemounts and counting of RGCs after exposure to ROCKis. **a** Representative images of wholemount retinal explants in culture at DEV 0 and control solvent DEV 4 or treated DEV 4 groups (500 µM Y-27632, 50 µM Y-33075, and 100 µM H-1152) immunolabeled with Brn3a at 20 × magnification (scale bar = 150 µm). **b** Quantification of Brn3a$^+$ RGCs (n = 9–24 per group, ****$p < 0.0001$) from wholemount retinal explants. Unpaired t tests or Mann–Whitney tests were performed between the control and each treated group at DEV 4. Error bars indicate the standard error of the mean

Differential analysis of gene expression in retinal explants treated with Y-33075

Y-33075 at 50 µM was the most effective ROCKi in protecting against RGC loss. Thus, we investigated the underlying neuroprotective and immunomodulatory mechanisms by analyzing transcriptomic differential gene expression. We performed RNA-seq on retinal explants treated with 50 µM Y-33075 and compared the

transcriptome with that of the control solvent group. The distribution of the gene expression of the samples under these two conditions is shown in Fig. 5a. Features with fewer than 500 counts were excluded, resulting in the detection of 23,098 genes. Among them, 131 showed significantly different expression between the two groups (adjusted *p*-value, padj < 0.05).

A volcano plot of the differentially expressed genes (DEGs) in the Y-33075 treated group versus the control solvent group is shown in Fig. 5b. Among the DEGs, 118 genes were downregulated in the Y-33075 treated condition, and 13 were upregulated.

Y-33075 significantly downregulates gene expression involved in inflammatory and cell death processes

The 25 most significantly downregulated genes in the Y-33075-exposed group ranked by the binary logarithm of fold change (log2FC). For each gene identifier, the name, log2FC, and adjusted *p*-value (padj) are presented.

Top 25 significantly downregulated genes in the Y-33075 group

The 25 most significantly downregulated genes in the Y-33075 treated group (Fig. 6a and Table 2) versus the control solvent group are involved in the complement activation and protein activation cascades (*C1qa*, *C1qb*, *C1qc*, and *Cfh*), microglial and glial cell activation and the neuroinflammatory response (*Tafa3*, *C1qa*, and *Cx3cr1*), the chronic inflammatory response (*Cx3cr1* and *Ccl2*), and microglial development and maintenance (*Csf1r*) (Fig. 6b) based on the GO database for biological process analysis.

Downregulation of glial and microglial cell markers

We investigated other genes of interest to corroborate the immunohistology analysis concerning microglial and glial cell markers and to investigate the inflammatory process, cell death, and the inflammasome at the transcriptomic level. RNA-seq data showed a significant decrease in the classical microglial markers *Cd11b* and *Cd68* and the glial marker *Gfap* between the DEV 4 control and Y-33075-treated groups (Fig. 6c). This decrease in immune cell marker expression after Y-33075 exposure was confirmed by RT-qPCR analysis for *Cd11b* and *Cd68*. There was no significant difference on DEV 4 between the control and treated groups for *Gfap* mRNA (Additional File 1A). These data corroborate and reinforce the immunohistology analyses, showing a significant effect of 50 µM Y-33075 on microglial proliferation and activation and limiting of astrogliosis at the protein and mRNA levels.

Downregulation of classical M1 gene expression markers

We investigated the expression of the classical M1 pro-inflammatory cytokines markers *Tnfa* and *Il1b* (Fig. 6d). *Tnfa* and *Il1b* gene expression was significantly lower in the Y-33075-exposed group than in the control solvent group at DEV 4. This downregulation of *Tnfa* and *Il1b* expression was confirmed by RT-qPCR analysis (Additional file 1B.)

Downregulation of inflammasome component markers

We studied the expression of genes involved in the NLRP1 and NLRP3 inflammasome pathways, which play a crucial role in glaucoma pathology, to determine the mechanism of action of the neuroprotection and immunomodulation induced by Y-33075 exposure (Fig. 6e). *Nlrp1a* was strongly downregulated in the treated group at DEV 4 following axotomy. *Nlrp3*, *Pycard*, and *Casp1*, three genes that code for proteins composing the NLRP3 inflammasome, were significantly downregulated after four days of Y-33075 exposure at 50 µM. The *Il18* gene, of which the protein pro-IL-18 is cleaved by active caspase-1, was also significantly downregulated after Y-33075 exposure.

Downregulation of apoptosis and ferroptosis markers

Finally, we studied the gene expression of *Casp3* and *Casp8* as intrinsic and extrinsic apoptosis markers and *Ptgs2* gene expression as a ferroptosis marker (Fig. 6f). These three genes were significantly downregulated at DEV 4 after Y-33075 exposure.

(See figure on next page.)

Fig. 3 Y-27632, Y-33075, and H-1152 prevent microglial cell proliferation and activation in wholemount retinal explants in culture. **a** Representative confocal images of wholemount retinal explants in culture at DEV 0 and for the control solvent DEV 4 and treated DEV 4 groups (50 µM Y-33075, 100 µM H-1152, and 500 µM Y-27632) immunolabeled with Iba1 (green) at 20 × magnification (n = 6 per group), scale bar = 150 µm. **b** Representative confocal images of retinal explant cryosections in culture at DEV 0 and for the control solvent DEV 4 and treated DEV 4 groups (50 µM Y-33075, 100 µM H-1152 100 µM and Y-27632 500 µM) immunolabeled with Iba1 (green) and CD68 (red) at 40 × magnification (n = 6 per group), scale bar = 100 µm. **(C)** Graph displaying the calculated percentages of microglial cells on viable cells ($CD11b^+$, $CD68^+$ and double $CD11b^+$/ $CD68^+$) labeled in explants at DEV 4 as determined by flow cytometry analysis. Unpaired t test or Mann–Whitney test were performed between the control and Y-33075-treated group at DEV 4 (n = 7–17/group, $*p < 0.05$, $****p < 0.0001$). Error bars indicate the standard error of the mean

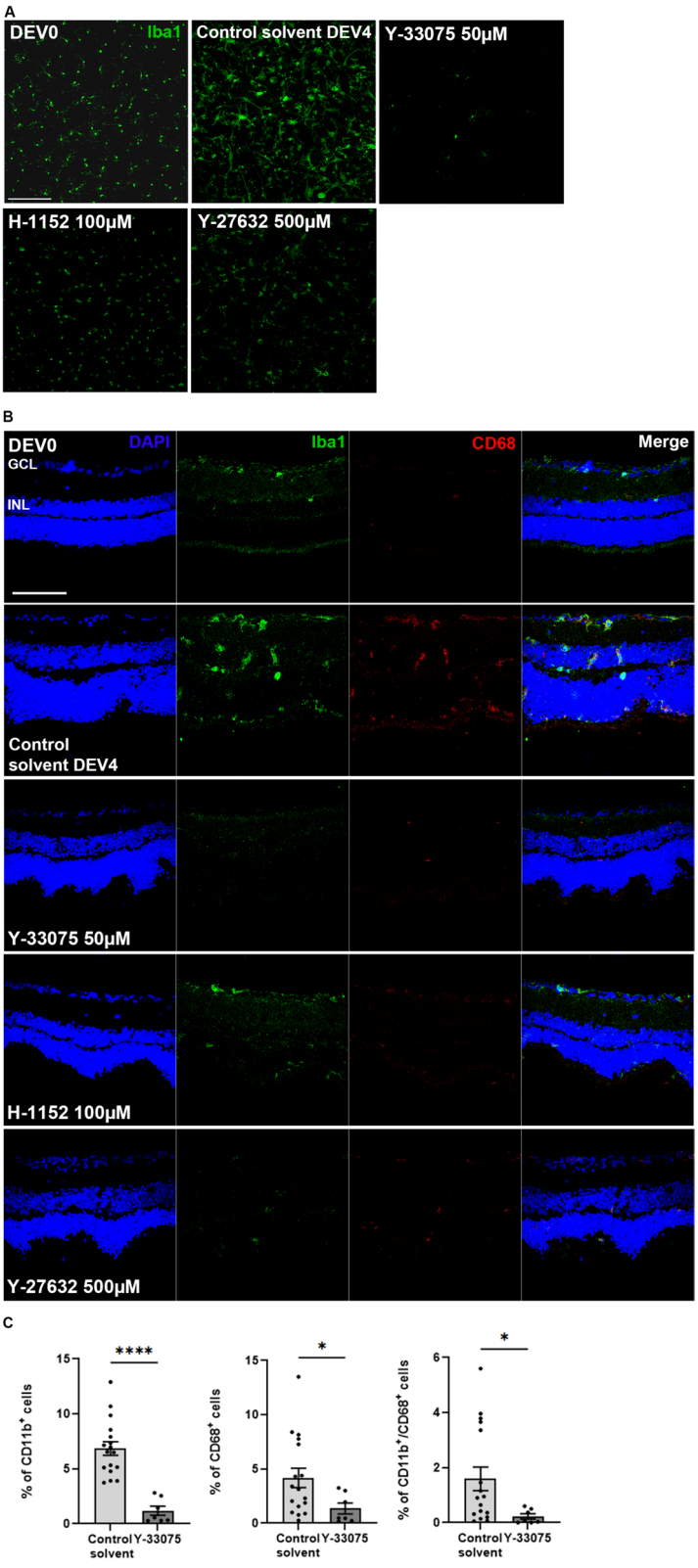

Fig. 3 (See legend on previous page.)

Downregulation of other genes of interest involved in the inflammation pathway or RGC function

We investigated the expression of other genes of interest involved in the inflammatory pathway or the maintenance of RGC function. They included *Tlr2, 3,* and *4* (Fig. 7a), the NF kappa b pathway genes *Nfkb1* and *2* for their role in the inflammatory activation pathway (Fig. 7b), and *P2rx7* as a mediator of proliferation and migration of retinal microglia, *Nos2* as a well-known pro-inflammatory mediator, and *Gpr84* as a proinflammatory receptor (Fig. 7c). The expression of all these genes was significantly downregulated by 50 µM Y-33075 after four days of culture.

Y-33075 significantly upregulates genes expressed by RGCs involved in neurotransmitter regulation

Top 13 significantly upregulated genes in the Y-33075 group

Among the 13 most highly upregulated genes (Table 3) after exposure to 50 µM Y-33075, we found neurofilament markers, including the *Nefh* (neurofilament heavy chain) gene, which is a direct neuronal marker, and the *Prph* (Peripherin) gene, which is expressed by photoreceptors. Other genes involved in the regulation of neurotransmitters, such as *Nrn1* (Neuritin1), of which the expression promotes RGC survival, and *Rbpms* (RNA binding protein mRNA processing factor) and *Slc17a6* (Solute carrier family 17 member 6), both RGC-specific markers, were also significantly upregulated (Fig. 8b).

Upregulation of the expression of other classical and specific RGC and neuronal genes after exposure to Y-33075

Finally, the neuronal marker *Thy1* and the RGC-specific marker *Pou4f1* were significantly upregulated in the treated group versus the control solvent group after four days of culture (Fig. 8c).

The schematic representation illustrates a potential mechanism by which the ROCK inhibitor Y-33075 protects against retinal ganglion cell (RGC) death. Optic nerve axotomy triggers RGC death through several mechanisms, including neuroinflammation, apoptosis, ferroptosis, and pyroptosis. The ROCK inhibitor Y-33075 promotes RGC survival by modulating these pathways. The green arrow indicates that Y-33075 reduces microglial and astrocyte activation (as evidenced by decreased CD68 + and IBA1 + cells, along with reduced GFAP immunoreactivity), diminishes M1 polarization, and downregulates the transcription of genes associated with apoptosis, ferroptosis, and pyroptosis (indicated in italics). In the diagram, green arrows represent activation/upregulation, while red arrows denote inhibition/downregulation.

Discussion

Numerous downstream elements of the ROCK pathway show high expression in the central nervous system, overseeing diverse neural processes, such as neuronal survival, axonal outgrowth, and guidance [38]. Given the substantial impact of Rho and ROCK on numerous cellular functions, focusing on this pathway is considered to be of value in addressing neurodegenerative diseases [26, 42, 43].

Previous studies have determined the action of ROCKis on the trabecular side of glaucomatous disease. Specifically, these compounds increase aqueous humor outflow by directly affecting the trabecular meshwork matrix and trabecular meshwork cell cytoskeleton [39, 40]. Although ROCKi drugs have been validated and commercialized for the treatment of ocular hypertension, their originality lies in their potential to directly act on the retinal side of the disease, in addition to their direct effects on the trabecular meshwork. There is increasing evidence that the Rho-ROCK pathway is involved in the pathophysiology of optic nerve damage in glaucoma, as ROCK is upregulated in the optic nerve head of glaucomatous patients [26, 41]. In addition, the topical administration of a ROCK/Net inhibitor has been demonstrated to promote the survival and regeneration of retinal ganglion cells following optic nerve injury [42]. For more than a decade, numerous experimental studies have investigated the effects of ROCKi in promoting neurite outgrowth, axonal regeneration, and reducing or stimulating gliosis in in-vitro models of RGC cultures, retinal explants, and after traumatic optic nerve lesions. These findings suggest that inhibiting ROCK may be a versatile strategy for treating glaucoma.

Here, we employed an ex-vivo model that involves axotomy and neuroretinal explants of rats. This model

(See figure on next page.)

Fig. 4 Y-33075 and H-1152 prevent astrogliosis in retinal explants. **a** Representative confocal images of retinal explant cryosections in culture at DEV 0 and for the control solvent DEV 4 and treated DEV 4 (50 µM Y-33075, 100 µM H-1152, and 500 µM Y-27632) groups immunolabeled with GFAP (green) at 40 × magnification (n = 6 per group). Scale bar = 100 µm. **b** *Gfap* gene expression analysis in retinal explants at DEV 0 and DEV 4. Unpaired t-test test was performed between the control solvent and each other group. Error bars represent the standard error of the mean. *$p < 0.05$, ***$p < 0.005$

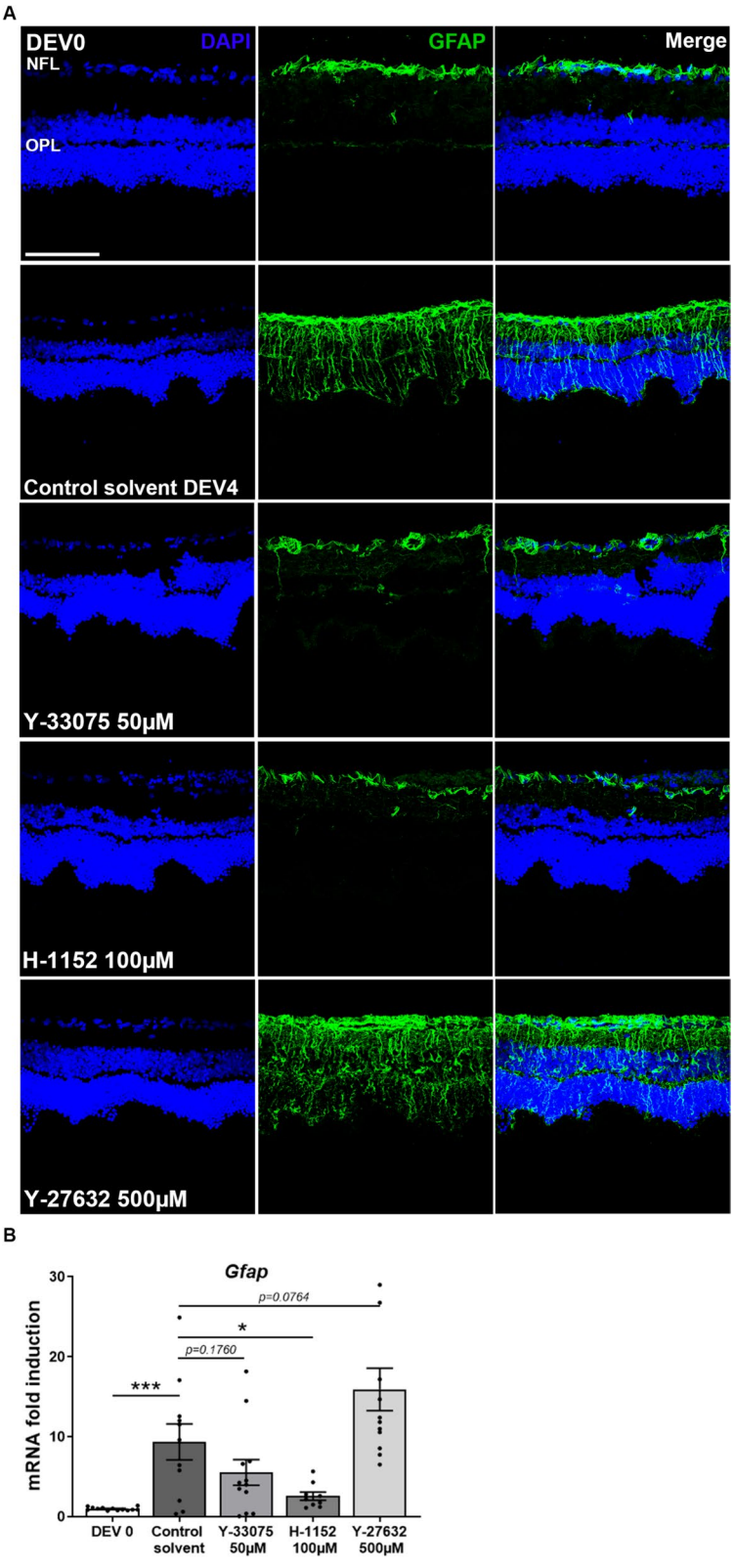

Fig. 4 (See legend on previous page.)

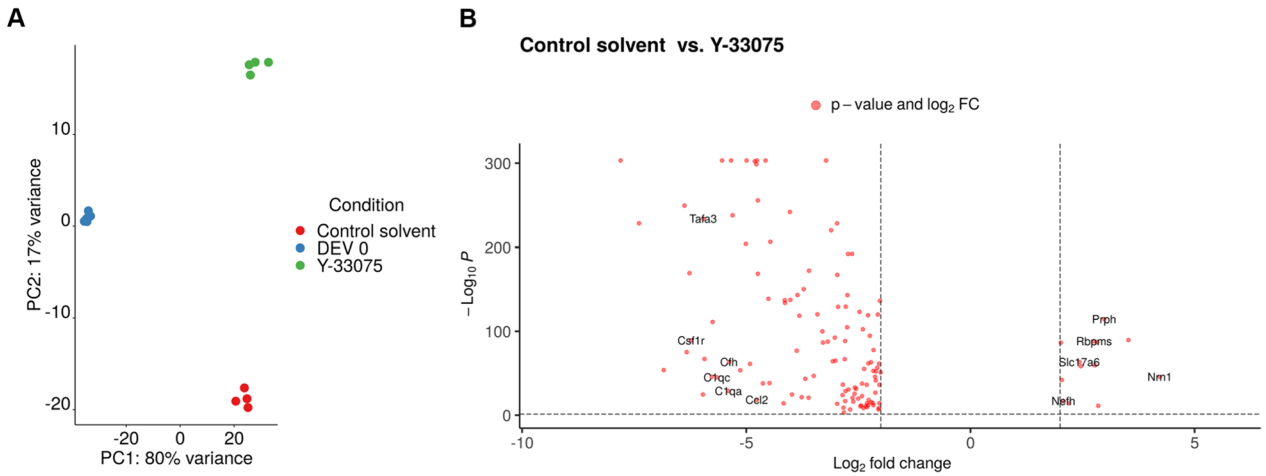

Fig. 5 RNA-seq analysis of DEV 0 and DEV 4 treated and untreated retinal explants. **a** Principal component analysis (PCA) plot of DEV 0 and DEV 4 control solvent and Y-33075 RNA-seq analysis illustrating the distribution of gene expression of the samples for the three conditions. **b** Volcano plot identifying the differentially expressed genes (DEGs) in the Y-33075 treated group versus the control solvent group. Red dots represent the 131 genes that were significantly differentially expressed (padj < 0.05) with a fold-change ≤ − 2 or ≥ + 2 (− 2 ≤ log2FC ≥ + 2), of which 118 were downregulated and 13 upregulated in the Y-33075 treated condition

offers distinct advantages over in vitro models that use cell lines or dissociated primary cells. Notably, it allows for the assessment of cellular effects with a multicellular response involving both neurons and glial cells. Importantly, this approach preserves the retinal tissue architecture, thus retaining the complexity of the effects arising from cellular interactions. Previous studies [32, 43] have validated these aspects, facilitating the experimental reproduction of two crucial features observed in glaucomatous optic neuropathy: the accelerated and irreversible degeneration of RGCs and the presence of proliferative and reactive glial cells that contribute to the local production of inflammatory factors [5, 6, 44]. Thus, this model provides an accurate means to reproducibly evaluate the neuroprotective, anti-inflammatory, and immunomodulatory potential of ROCKis. It offers these insights without investment of the time and resources required for establishing an in-vivo model, while also minimizing the number of animals euthanized.

The primary goal of this study was to evaluate the effectiveness of three ROCKis (Y-27632, Y-33075, and H-1152) in modulating the molecular and cellular mechanisms that promote the survival of retinal ganglion cells (RGCs) and reduce retinal inflammation. We examined tissue transcriptomes and determined gene expression patterns using RNA-seq following treatment of retinal explants with the ROCKi that showed the most potent neuroprotective effects. This approach proved to be robust in pinpointing differentially expressed genes, uncovering novel transcripts, and providing insights into the functional roles of genes within these biological processes. Subsequently, we adopted a connectome approach to elucidate the connectivity patterns and interactions among distinct mRNA molecules involved in cellular communication and signaling pathways.

The three compounds used in the present study, Y-27632, Y-33075, and H-1152, have already been shown to have a potential dual mechanism of action, both trabecular and neuroprotective [28, 45–49]. However, they

(See figure on next page.)

Fig. 6 Analysis of downregulated genes in Y-33075-exposed retinal explants. **a** Heatmap showing the response to treatment corresponding to the control solvent or Y-33075 and the variability of expression for each sample for the 25 most significantly downregulated genes in the Y-33075 group versus the control solvent group. **b** RNA-seq-based read count plot gene expression analysis of the TOP 25 downregulated genes in retinal explants at DEV 0 and DEV 4. **c** RNA-seq-based read count plot gene expression analysis of microglial and glial cell markers in retinal explants at DEV 0 and DEV 4. **d** RNA-seq based read count plot gene expression analysis of M1 inflammatory markers in retinal explants at DEV 0 and DEV 4. **e** Read count plots of the inflammasome component gene markers *Nlrp1*, *Nlrp3*, *Pycard*, and *Casp1* and their downstream targets Il1b and *Il18* in retinal explants at DEV 0 and DEV 4. **f** Read count plots of the apoptosis gene markers *Casp3* and *Casp8* and the ferroptosis gene marker *Ptgs2* in retinal explants at DEV 0 and DEV 4. Unpaired t tests or Mann–Whitney tests were performed between the control solvent and 50 µM Y-33075-treated groups at DEV 4. Error bars indicate the standard error of the mean. *$p < 0.05$, **$p < 0.01$, ***$p < 0.001$, ****$p < 0.0001$)

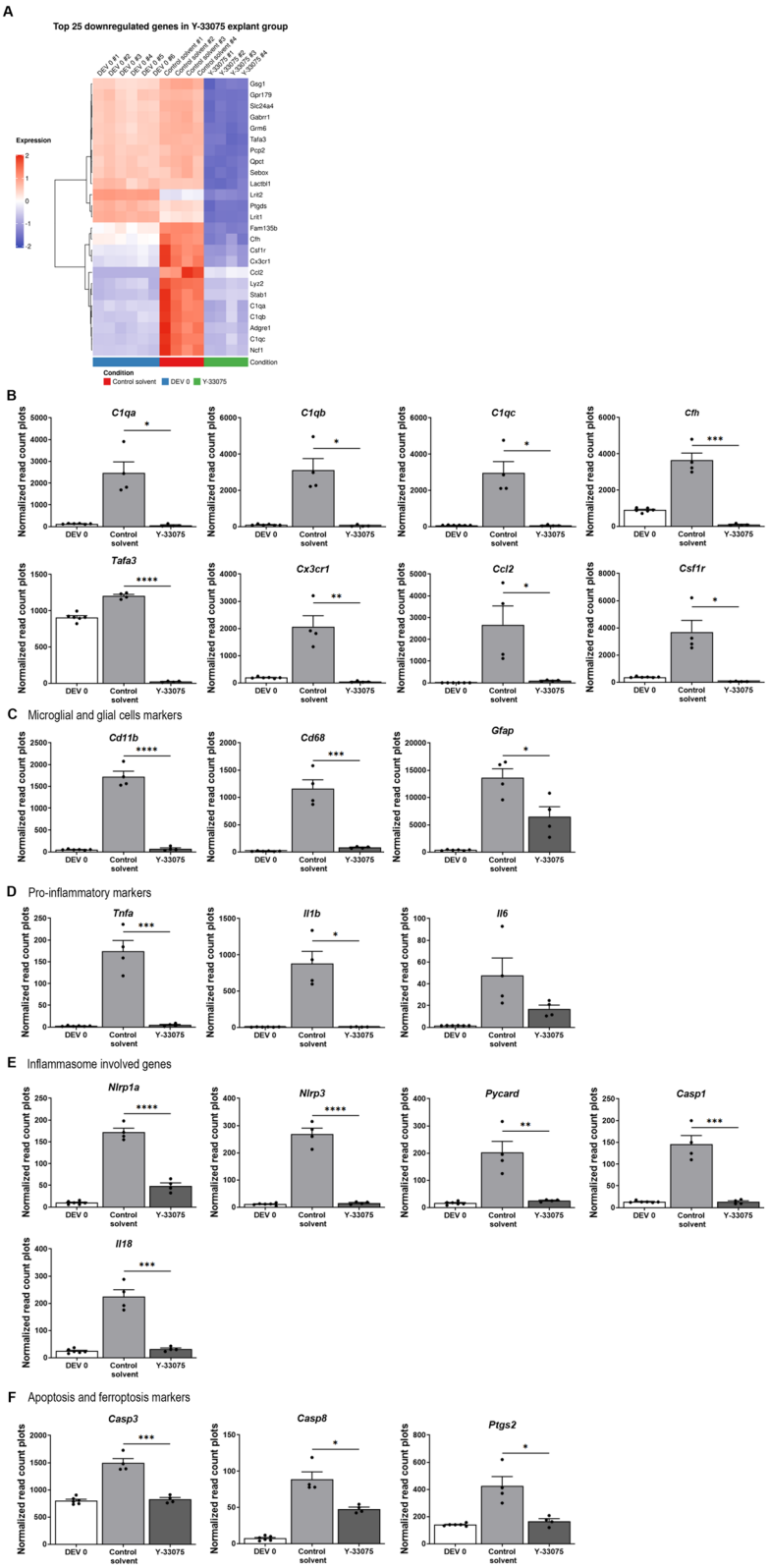

Fig. 6 (See legend on previous page.)

Table 2 Top 25 downregulated genes in the Y-33075-treated group versus the control solvent group

Gene ID	Gene name	log_2 Fold Change	padj
Ccl2	C–C motif chemokine ligand	− 4.767	4.64E-19
Qpct	Glutaminyl-peptide cyclotransferase	− 4.774	2.20E-299
Fam135b	Family with sequence similarity 135, member B	− 4.811	6.41E-303
Stab1	Stabilin 1	− 4.916	6.31E-62
Slc24a4	Solute carrier family 24 member 4	− 4.994	0.00E + 00
Gpr179	G protein-coupled receptor 179	− 5.01	1.15E-204
Lyz2	Lysozyme 2	− 5.135	2.76E-54
Sebox	SEBOX homeobox	− 5.306	1.39E-238
Gabrr1	Gamma-aminobutyric acid type A receptor subunit rho 1	− 5.339	0.00E + 00
Cfh	Complement factor H	− 5.384	3.97E-64
C1qa	Complement C1q A chain	− 5.399	1.25E-29
Grm6	Glutamate metabotropic receptor 6	− 5.54	0.00E + 00
C1qc	Complement C1q C chain	− 5.657	7.41E-46
Gsg1	Germ cell associated 1	− 5.751	7.46E-112
Cx3cr1	C-X3-C motif chemokine receptor 1	− 5.772	1.55E-46
Lrit2	Leucine-rich repeat, Ig-like and transmembrane domains 2	− 5.932	8.24E-68
Tafa3	TAFA chemokine like family member 3	− 5.963	1.40E-234
C1qb	Complement C1q B chain	− 5.967	1.89E-25
Csf1r	Colony stimulating factor 1 receptor	− 6.232	6.17E-90
Lactbl1	Lactamase beta like 1	− 6.266	5.21E-170
Ncf1	Neutrophil cytosolic factor 1	− 6.329	6.25E-76
Ptgds	Prostaglandin D2 synthase	− 6.378	3.55E-250
Adgre1	Adhesion G protein-coupled receptor E1	− 6.841	1.44E-54
Pcp2	Purkinje cell protein 2	− 7.392	4.28E-229
Lrit1	Leucine-rich repeat, Ig-like and transmembrane domains 1	− 7.804	0

differ mainly in their therapeutic target and inhibitory potential. Y-27632 was one of the first ROCKis to be developed and inhibits both isoforms of Rho kinases, whereas H-1152 specifically targets ROCK2, the most highly expressed isoform in the central nervous system [50]. In addition, Y-33075 (or Y-39983) appeared to be of particular interest because of its very high inhibition potential, more than 20 times greater than that of Y-27632 [51]. The mechanisms of action of Y-33075 are still relatively unknown, unlike those of Y-27632 and H-1152, probably due to the lower specificity of Y-33075 for Rho kinase activity, the minimal inhibitory concentration of Y-33075 for protein kinase C and calmodulin-dependent protein kinase II being lower than that of the other ROCKis. Thus, this molecule appeared to be a weaker candidate for exploring the specific biological effects of ROCK pathway inhibition [52].

In this study, only the ROCKi Y-33075 showed a significant effect on RGC survival at a concentration of 50 µM on DEV 4. Few studies have investigated the efficacy of Y-33075 on RGC survival, with inconsistent results. In the study of Sagawa et al., exposure to Y-33075 in an ex-vivo model of neuroretinal explants from adult cats showed no significant effect on RGC survival [53]. In another study based on an in-vivo rat model of optic nerve crush, RGC density was significantly higher in rats exposed to ROCKis [54]. RNA-seq analysis carried out in our study revealed the upregulation of genes specifically expressed by RGCs in the neuroretina (*Rbpms*, *Pou4f1* and *Slc17a6*) and by neurons (*Thy1*), confirming the efficacy of Y-33075, even in the acute model of optic nerve axotomy. In addition, the same analysis showed that the expression of gene markers of neurofilaments (*Nrn1*, *Nefh*) and a photoreceptor marker (*Prph*) were much higher in treated explants than in controls. Although we did not specifically analyze the quantitative and qualitative evolution of neurites, these results are consistent with those of previous studies showing that Y-33075 promotes neurite formation and growth [53–55]. Y-33075 therefore appears to be effective in promoting RGC survival while also acting on the dynamic metabolism of neurites.

On the other hand, several studies have demonstrated the efficacy of H-1152 and Y27632 in reducing RGC apoptosis [29, 45, 56, 57]. Exposure to these molecules at comparable concentrations in our ex-vivo model showed

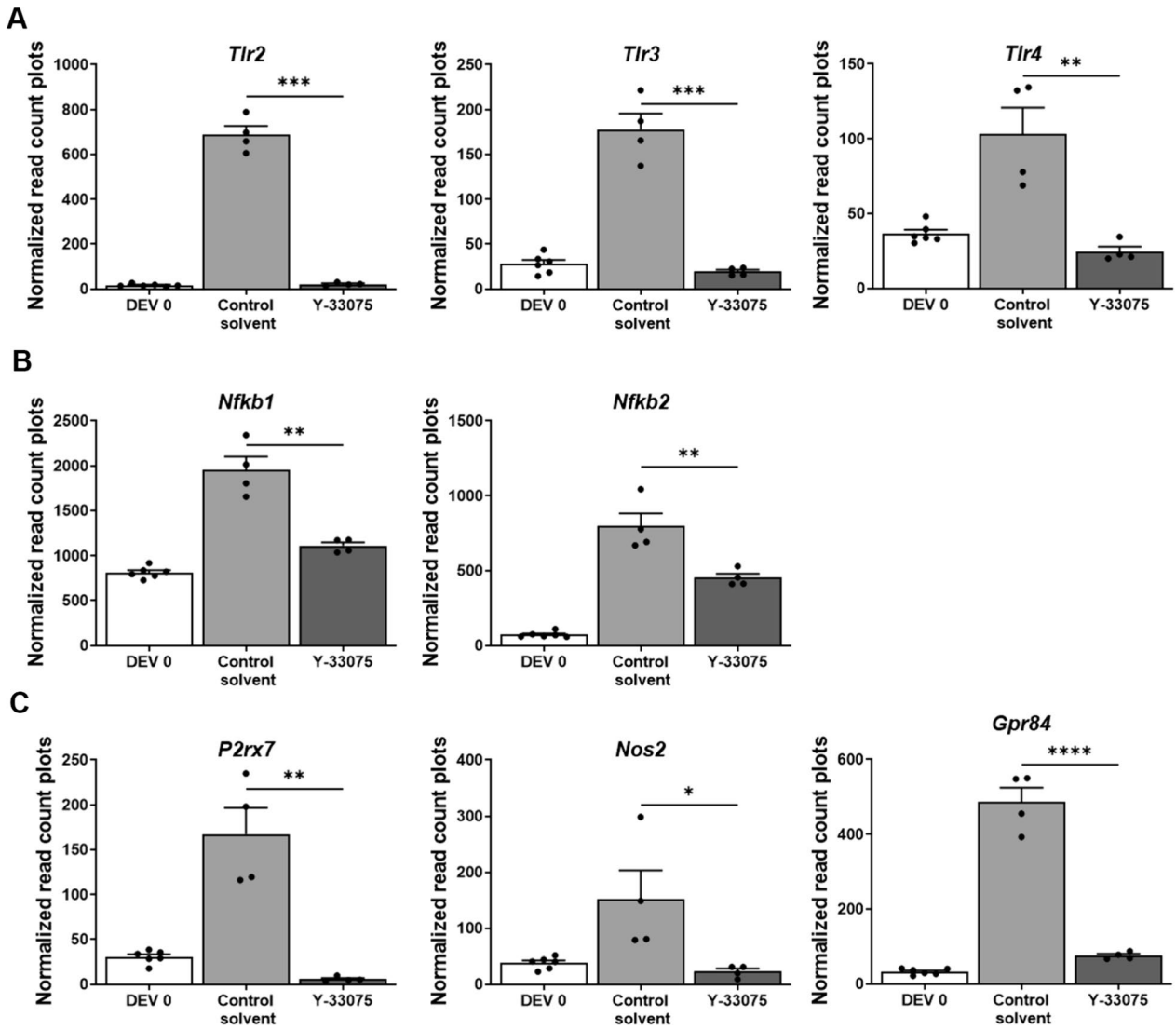

Fig. 7 Analysis of other genes of interest downregulated by Y-33075. RNA-seq-based read count plot gene expression analysis of *Tlr2*, *Tlr3*, and *Tlr4* (**a**), *Nfkb1* and *Nfkb2* (**b**), and *P2rx7*, *Nos2*, and *Gpr84* genes (**c**) in retinal explants at DEV 0 and DEV 4. Unpaired t tests or Mann–Whitney tests were performed between the control solvent and the 50 µM Y-33075 treated groups at DEV 4. Error bars represent the standard error of the mean. *$p < 0.05$, **$p < 0.01$, ***$p < 0.001$, ****$p < 0.0001$)

no efficacy on RGC survival, despite using relatively high concentrations and H-1152 does indeed exhibit a distinct anti-gliosis effect (Figs. 3 and 4), but this effect alone does not appear to be sufficient to protect retinal ganglion cells (RGCs) from death. Therefore, we cannot rule out the possibility that a direct effect on RGCs, such as anti-apoptotic or anti-ferroptotic mechanisms, may be necessary, at least in part, for their protection. The death of RGCs following optic nerve axotomy is driven by a combination of interconnected factors, including but not limited to the glial response. Other key contributors to this complex process include loss of trophic support, oxidative stress, axonal degeneration, apoptotic pathways, and ferroptosis, among others and still debated process.

Also, these results could be due to the variability of RGC responses evaluated in different models and therapeutic windows. However, we previously demonstrated the sensitivity of our model to reference neuroprotective molecules such as BDNF [32, 58]. We can thus affirm that these two ROCKis had a weaker neuroprotective effect than Y-33075 under our study conditions.

Thus, Y-33075 was more effective than the other ROCKis on RGC survival. This effect can be explained by

Table 3 Top 13 upregulated genes in the Y-33075 treated group versus the control solvent group

Gene ID	Gene name	log_2 Fold change	padj
Nrn1	Neuritin 1	4.223	1.47E-46
Ciart	Circadian associated repressor of transcription	3.523	2.64E-90
Prph	Peripherin	2.983	3.16E-115
Lamb3	Laminin subunit beta 3	2.851	5.50E-12
Trarg1	Trafficking regulator of GLUT4	2.826	9.82E-88
Rbpms2	RNA binding protein mRNA processing factor 2	2.777	2.96E-60
Rbpms	RNA binding protein mRNA processing factor	2.757	5.99E-89
Tppp3	Tubulin polymerization-promoting protein family member 3	2.463	4.75E-59
Slc17a6	Solute carrier family 17 member 6	2.429	3.56E-64
Fosl1	FOS like 1 AP-1 transcription factor subunit	2.198	6.58E-15
Nefh	Neurofilament heavy chain	2.074	1.08E-17
Rgs5	Regulator of G-protein signaling 5	2.037	9.56E-43
Nell2	Neural EGFL like 2	2.016	3.08E-87

Upregulated genes in the Y-33075 exposed group at DEV 4 versus the control solvent group ranked by the binary logarithm of fold change (log2FC). For each gene identifier, the name, log2FC, and adjusted *p*-value (padj) are presented.

its much higher inhibitory potential than the others, as well as by the recruitment of other protein kinases (protein kinase C and calmodulin-dependent protein kinase II). The results of this study do not allow us to conclude with certainty about the mechanisms involved. However, RNA-seq analysis identified strong downregulation of certain gene markers of apoptosis (*Casp3* and *Casp8*) and ferroptosis-related genes (*Ptgs2*) in Y-33075-exposed explants [59, 60]. The neuroprotective efficacy of ROCKis could therefore be mediated by the direct modulation of apoptosis or ferroptosis signals. Indeed, numerous studies have highlighted the importance of ROCK in cell death signaling in different models of neuronal injury, via, for example, increased activity of the PTEN pathway or the p38/MAP kinase pathway [61, 62]. However, given the complexity of the mechanisms involved in the onset of RGC degeneration in glaucoma, it is improbable that this mechanism alone accounts for the neuroprotective effects induced by Y-33075.

As previously mentioned, glaucomatous optic neuropathy, as well as preclinical models of glaucoma in rodents, is characterized by the activation and proliferation of microglial and astrocytic cells in the neuroretina, which are responsible for the release of cytokines and chemokines involved in RGC loss [5]. Microglial cells exist in two active forms with antagonistic effects: the neurotoxic pro-inflammatory M1 or "classical" activation state and the neuroprotective M2 or "alternative" activation state [15, 63, 64]. During RGC degeneration, the M1 state of microglia is particularly involved, notably by leading to the production of pro-inflammatory factors such as TNFα, IL-1β, and IL-6. Reducing the activation of these pro-inflammatory microglial cells could therefore be a significant therapeutic target. Inhibition of the ROCK pathway appears to be particularly promising. In addition to being involved in the morphological and functional regulation of RGCs, it is also critical for the production of these inflammatory phenomena, in particular, for the induction of the M1 profile of microglia, the release of inflammatory cytokines, and the production of astrocytic gliosis [65]. In our study, we were able to assess the effects of ROCKis on the activity and morphology of microglial cells and astrocytes. In addition, exposing explants to ROCKis led to a reduction in microglial cell proliferation, as shown by $Iba1^+$ immunostaining and FACS analysis of $CD11b^+$ and $CD68^+$ for Y-33075. There was also a qualitative and quantitative decrease in microglial cell activation ($Iba1^+/CD68^+$ and

(See figure on next page.)

Fig. 8 Analysis of upregulated genes in Y-33075 exposed retinal explants. **a** Heatmap depicting the treatment response to either the control solvent or Y-33075, along with the expression variability for each sample among the 13 significantly upregulated genes in the Y-33075 group compared to the control solvent group. **b** Read count plots for the neurofilament gene markers Nefh and Prph, the neurotransmitter gene marker Nrn1, and the RGC-specific gene markers Rbpms and Slc17a6 in retinal explants at DEV 0 and DEV 4, which are among the top 13 most highly expressed genes. **c** Read count plots of the RGC-specific gene marker *Pou4f1*, the neuronal gene *Thy1* in retinal explants at DEV 0 and DEV 4. Unpaired t tests or Mann–Whitney tests were performed between the control solvent and 50 µM Y-33075-treated groups at DEV 4. Error bars indicate the standard error of the mean. *$p < 0.05$, ***$p < 0.001$, ****$p < 0.0001$)

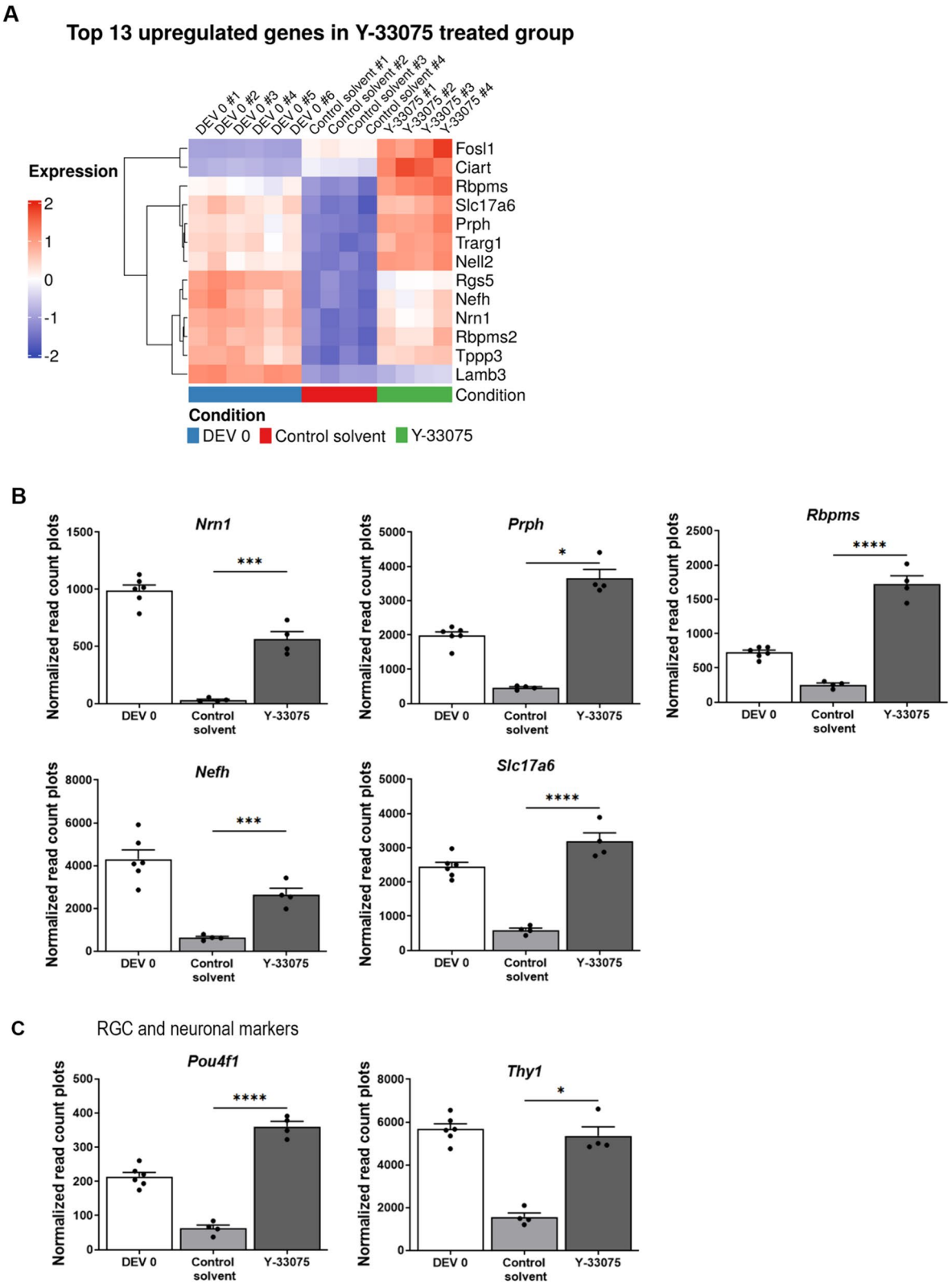

Fig. 8 (See legend on previous page.)

$CD11b^+/CD68^+$ cells) and a reduction in astrocytic infiltration throughout the retina. These results have been relatively well documented for H-1152 and Y-27632 [26, 29]. By contrast, only one study had previously reported the activity of the ROCKi Y-33075 on retinal gliosis. Y-33075 appeared to reduce the extension of glial processes in the ex-vivo model of neuroretinal explants from cats [53]. To gain a better understanding of its still relatively unknown anti-inflammatory effects, we carried out a transcriptomic analysis on explants exposed to 50 µM Y-33075 compared to those treated with the control solvent. RNA-seq, validated for certain classical study genes by RT-qPCR analysis, confirmed previous findings, showing downregulation of the transcription of pro-inflammatory factors for the M1 state of microglia (*Tnfα* and *Il1b*) and the glial cell markers *Cd11b*, *Cd68*, and *Gfap*. Other factors associated with the activation (*Tafa3*, *C1qa* and *Cx3cr1*) and development and maintenance (*Csf1r*) of these cells were downregulated. Y-33075 therefore appears to have anti-inflammatory and immunomodulatory activity, notably by regulating the proliferation and activation of microglial and astrocytic cells. In addition, transcriptional analysis identified a decrease in gene expression of many other pro-inflammatory factors, including those of the classical complement activation pathway (*C1qa*, *C1qb*, *C1qc*, and *Cfh*). A similar finding was reported in a recent study in which inhibition of the Rho kinase pathway induced inactivation of the classical complement pathway [66]. Moreover, C1q has recently been identified as one of the upregulated cofactors in the retinas of animal models of glaucoma [67]. However, its activity is highly complex. On the one hand, it promotes the survival of RGCs by indirectly regulating their electrical activity while inducing the opsonization of apoptotic RGCs. The benefit of the reduction in gene expression of the C1q fraction of complement on RGCs found in our study is, therefore, debatable. Further studies will be required to assess the effects of ROCKi modulation of the classical complement pathway on the evolution of inflammatory parameters in models of RGC inflammation and degeneration. The expression of components of the inflammasome (*Nlrp1*, *Nlrp3*, *Pycard* and *Casp1*) and its targets (*Il1b* and *Il18*) has been studied to determine the action mechanism of neuroprotection and immunomodulation induced by Y-33075 exposure [68]. Indeed, the inflammasome and its targets play a crucial role in glaucoma pathology. Its activation is promoted by caspase-8 expression, which has been shown to promote NLRP1/NLRP3 inflammasome activation and IL-1β production in acute glaucoma. These factors were strongly downregulated after Y-33075 exposure following axotomy. The *Nlrp3*, *Pycard*, *Casp1*, and *Il18* genes, of which the protein pro-IL-18 is cleaved by active caspase-1, thus triggering the inflammatory response, was also significantly downregulated by Y-33075 exposure. These findings are consistent with the results of a study demonstrating that exposure to ROCKis significantly decreases IL-1β and caspase-1 production [69]. The involvement of the NLRP3 inflammasome in the induction of RGC degeneration by pyroptosis in experimental glaucoma models has also been suggested by a recent study [70]. IL-1β could, therefore, play a key role in the pathogenesis of glaucoma, at the crossroads of neuroinflammation and pyroptosis. It is highly probable that inhibition of the production of such a molecule by Y-33075 plays a fundamental role in protecting RGCs, along with its anti-apoptotic and retinal anti-inflammatory effects. We also investigated other genes of interest differentially expressed by glaucoma patients. The *Tlr 2, 3, and 4* genes, for which anatomical studies have shown increased microglial and glial expression in the retinas of glaucoma patients [71], were strongly downregulated by Y-33075. Activation of the TLR pathway, leading to increased expression of proinflammatory proteins via the NFkb pathway, of which the *Nfkb1* and *2* genes were also downregulated in our study, provides an indication of the mode of action of Y-33075 in immunomodulation. The purinergic receptor P2RX7 gene, which was significantly downregulated in our model following Y-33075 exposure, has been identified as a potent mediator of retinal microglia proliferation and migration, and its role in inflammasome activation is well documented. More specifically, its role in retinal diseases, such as glaucoma, age-related macular degeneration (AMD), and uveitis, has been thoroughly reviewed [72, 73]. P2RX7 is involved in the release of the pro-inflammatory cytokines IL-1β and IL-18 by activating the inflammasome NLRP3 and TNFα after stimulation by ATP [74]. Sanderson et al. also demonstrated that stimulation of P2X7R by the agonist BzATP (100 µM) in human organotypic retinal cultures induces the loss of RGC markers and mediates RGC death [75]. It could therefore be a powerful therapeutic target in ocular diseases. NOS-2, a well-known proinflammatory mediator activated by TNFα, is also overexpressed in the optic nerve head of glaucomatous donors [76]. Yuan et al. investigated the expression of pro-inflammatory markers in optic nerve heads of human glaucomatous donor eyes and those from donors with no recorded ocular disease. This study showed NOS-2 expression to be markedly higher than that in normal patient optic nerve heads in the prelaminar regions and *lamina cribosa* of the optic nerve head, reactive astrocytes, and parenchymal microglia in advanced glaucoma. Consistent with our RNA-seq results showing the downregulation of *Tnfa*, *Nos-2* was also significantly downregulated by Y-33075 in our model. Finally, GPR84, already known to be a

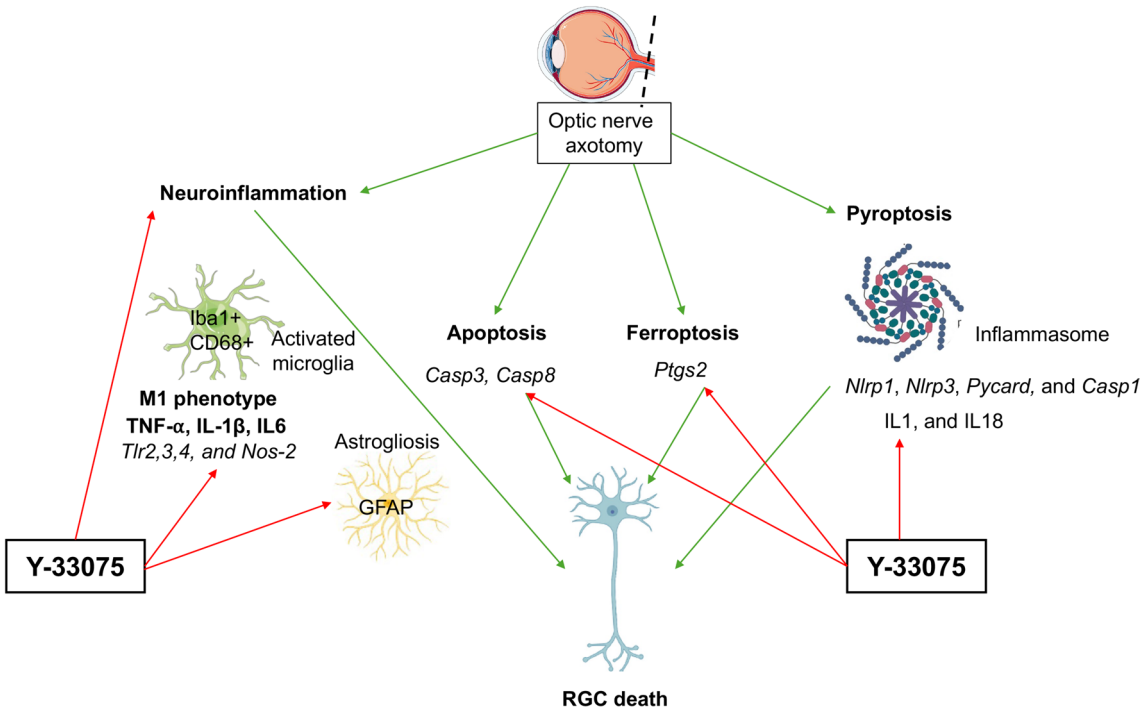

Fig. 9 Schematic representation of a potential mechanism by which the ROCK inhibitor Y-33075 protects against retinal ganglion cell (RGC) death

pro-inflammatory receptor, was recently identified as a mediator of a subpopulation of microglial cells that promotes TNF/IL-1α expression [30]. Using transcriptomic analysis, Sato et al. observed that a particularly cytotoxic form of microglia that promotes TNF/IL-1α expression showed high GPR84 positivity in an optic nerve crush model. They evaluated the anti-neuroinflammatory effects and modulation of *Gpr84* expression induced by the ROCKi ripasudil and concluded that Rho kinase activation is a key event in the development of GPR84^{high} neurotoxic microglial polarization. Our RNA-seq data showed the downregulation of *Gpr84* after Y-33075 exposure, in accordance with the downregulation of *Tnfa* and other pro-inflammatory markers.

Conclusion

This study demonstrates the neuroprotective potential of the ROCK inhibitor Y-33075 through its effectiveness in rescuing RGCs and its anti-inflammatory and immunomodulatory properties (Fig. 9, schematic representation of a potential mechanism by which the ROCK inhibitor Y-33075 protects against RGC death). This dual mechanism of action offers hope for the development of neuroprotective therapies for glaucoma. The involvement of multiple signaling pathways helps to address the complexity of RGC degeneration. However, further research is needed to fully understand the mechanisms of action of this potent ROCKi.

Abbreviations

BSA	Bovine serum albumin
DPBS	Dulbecco's phosphate buffer saline
DEV	Days ex vivo
GCL	Ganglion cell layer
GTP	Guanosine triphosphate
INL	Inner nuclear layer
IPL	Inner plexiform layer
NFL	Nerve fiber layer
ONL	Outer nuclear layer
OPL	Outer plexiform layer
PTFE	Polytetrafluoroethylene
RGC	Retinal ganglion cells
ROS	Reactive oxygen species
RT	Room temperature

Acknowledgements

We thank Stéphane Fouquet and Marie-Laure Niepon from the Image platform at the Sorbonne Université, Institut de la Vision, Paris, France. This work benefited from equipment and services from the iGenSeq core facility (Genotyping and sequencing) at ICM. We thank Xavier Guillonneau and Frédéric Blond from the Institut de la Vision for their contribution in RNA-seq data extraction and analysis. We would like to thank the Phénotypage Cellulaire et Tissulaire platform of the Institut de la Vision for the flow cytometry analysis.

Author contributions

ER, PB, AC, CD, and IB performed, analyzed, and interpreted the experiments. ER, PB, and SMK wrote the manuscript. ARLG, CO, CB, and SMK made substantial contributions to the conception and design of the study. CB, SMP, and JB supervised the study. All authors read and approved the final manuscript.

Funding

This work was funded by IHU FOReSight and an unrestricted grant from the Laboratoires Théa and from the Fondation des Aveugles de Guerre.

Availability of data and materials
The datasets used and/or analyzed during the current study are included in this published article or are available from the corresponding author upon reasonable request.

Declarations

Ethics approval and consent to participate
All experiments were conducted after evaluation and approval by the Institutional Animal Care and Use Committee in accordance with the guidelines of Directive 2010/63/EU of the European Parliament on the protection of animals used for scientific purposes.

Consent for publication
Not applicable.

Competing interests
Céline Olmière: employee of the Laboratoires Théa. Christophe Baudouin: Financial support and consultant (Alcon, Allergan; Santen, Laboratoires Théa). No competing interest to declare for the other authors.

Author details
[1]INSERM UMR 968, CNRS UMR 7210, Institut de la Vision, IHU FOReSIGHT, Sorbonne Université UM80, 75012 Paris, France. [2]Laboratoire, Quinze-Vingts National Ophthalmology Hospital, 75012 Paris, France. [3]INSERM-DHOS CIC 1423, IHU FOReSIGHT, Quinze-Vingts National Ophthalmology Hospital, 75012 Paris, France. [4]Faculty of Pharmacy of Paris, University Paris Cité, 75006 Paris, France. [5]Department of Ophthalmology III, Quinze-Vingts National Ophthalmology Hospital, IHU FOReSIGHT, 75012 Paris, France. [6]Department of Ophthalmology, Ambroise Paré Hospital, AP-HP, UVSQ, Paris Saclay University, 91190 Gif-sur-Yvette, France. [7]Laboratoires THEA, Clermont-Ferrand, France.

Received: 25 June 2024 Accepted: 31 August 2024
Published online: 14 September 2024

References

1. Jayaram H, Kolko M, Friedman DS, Gazzard G (2023) Glaucoma: now and beyond. Lancet 402(10414):1788–1801
2. Weinreb RN, Aung T, Medeiros FA (2014) The pathophysiology and treatment of glaucoma: a review. JAMA 311(18):1901–1911
3. Mohan N, Chakrabarti A, Nazm N, Mehta R, Edward DP (2022) Newer advances in medical management of glaucoma. Indian J Ophthalmol 70(6):1920–1930
4. Salvetat ML, Pellegrini F, Spadea L, Salati C, Zeppieri M (2023) Pharmaceutical approaches to normal tension glaucoma. Pharmaceuticals (Basel) 16(8):1172
5. Baudouin C, Kolko M, Melik-Parsadaniantz S, Messmer EM (2021) Inflammation in glaucoma: from the back to the front of the eye, and beyond. Prog Retin Eye Res 83:100916
6. Mélik Parsadaniantz S, Réaux-le Goazigo A, Sapienza A, Habas C, Baudouin C (2020) Glaucoma: a degenerative optic neuropathy related to neuroinflammation? Cells 9(3):535
7. Jassim AH, Inman DM, Mitchell CH (2021) Crosstalk between dysfunctional mitochondria and inflammation in glaucomatous neurodegeneration. Front Pharmacol 12:699623
8. Sapienza A, Raveu AL, Reboussin E, Roubeix C, Boucher C, Dégardin J et al (2016) Bilateral neuroinflammatory processes in visual pathways induced by unilateral ocular hypertension in the rat. J Neuroinflamm 13:44
9. Adornetto A, Russo R, Parisi V (2019) Neuroinflammation as a target for glaucoma therapy. Neural Regen Res mars 14(3):391–394
10. Wei X, Cho KS, Thee EF, Jager MJ, Chen DF (2019) Neuroinflammation and microglia in glaucoma: time for a paradigm shift. J Neurosci Res 97(1):70–76
11. Quaranta L, Bruttini C, Micheletti E, Konstas AGP, Michelessi M, Oddone F et al (2021) Glaucoma and neuroinflammation: an overview. Surv Ophthalmol 66(5):693–713
12. Tezel G (2022) Molecular regulation of neuroinflammation in glaucoma: current knowledge and the ongoing search for new treatment targets. Prog Retin Eye Res 87:100998
13. Ramirez AI, de Hoz R, Salobrar-Garcia E, Salazar JJ, Rojas B, Ajoy D et al (2017) The role of microglia in retinal neurodegeneration: Alzheimer's disease, parkinson, and glaucoma. Front Aging Neurosci 9:214
14. Miao Y, Zhao GL, Cheng S, Wang Z, Yang XL (2023) Activation of retinal glial cells contributes to the degeneration of ganglion cells in experimental glaucoma. Prog Retin Eye Res 93:101169
15. Tang Y, Le W (2016) Differential roles of M1 and M2 microglia in neurodegenerative diseases. Mol Neurobiol 53(2):1181–1194
16. Paolicelli RC, Sierra A, Stevens B, Tremblay ME, Aguzzi A, Ajami B et al (2022) Microglia states and nomenclature: a field at its crossroads. Neuron 110(21):3458–3483
17. Wang SK, Cepko CL (2022) Targeting microglia to treat degenerative eye diseases. Front Immunol 13:843558
18. Wang JW, Chen SD, Zhang XL, Jonas JB (2016) Retinal microglia in glaucoma. J Glaucoma 25(5):459–465
19. Berrino E, Supuran CT (2019) Rho-kinase inhibitors in the management of glaucoma. Expert Opin Ther Pat 29(10):817–827
20. Saha BC, Kumari R, Kushumesh R, Ambasta A, Sinha BP (2022) Status of Rho kinase inhibitors in glaucoma therapeutics-an overview. Int Ophthalmol 42(1):281–294
21. Al-Humimat G, Marashdeh I, Daradkeh D, Kooner K (2021) Investigational Rho kinase inhibitors for the treatment of glaucoma. J Exp Pharmacol 13:197–212
22. Schehlein EM, Robin AL (2019) Rho-associated kinase inhibitors: evolving strategies in glaucoma treatment. Drugs 79(10):1031–1036
23. Koch JC, Tatenhorst L, Roser AE, Saal KA, Tönges L, Lingor P (2018) ROCK inhibition in models of neurodegeneration and its potential for clinical translation. Pharmacol Ther 189:1–21
24. Chong CM, Ai N, Lee SMY (2017) ROCK in CNS: different roles of isoforms and therapeutic target for neurodegenerative disorders. Curr Drug Targets 18(4):455–462
25. Aguilar BJ, Zhu Y, Lu Q (2017) Rho GTPases as therapeutic targets in Alzheimer's disease. Alzheimers Res Ther 9(1):97
26. Van de Velde S, De Groef L, Stalmans I, Moons L, Van Hove I (2015) Towards axonal regeneration and neuroprotection in glaucoma: Rho kinase inhibitors as promising therapeutics. Prog Neurobiol 131:105–119
27. Raad M, El Tal T, Gul R, Mondello S, Zhang Z, Boustany RM et al (2012) Neuroproteomics approach and neurosystems biology analysis: ROCK inhibitors as promising therapeutic targets in neurodegeneration and neurotrauma. Electrophoresis 33(24):3659–3668
28. Alt A, Hilgers RD, Tura A, Nassar K, Schneider T, Hueber A et al (2013) The neuroprotective potential of Rho-kinase inhibition in promoting cell survival and reducing reactive gliosis in response to hypoxia in isolated bovine retina. Cell Physiol Biochem 32(1):218–234
29. Tura A, Schuettauf F, Monnier PP, Bartz-Schmidt KU, Henke-Fahle S (2009) Efficacy of Rho-kinase inhibition in promoting cell survival and reducing reactive gliosis in the rodent retina. Invest Ophthalmol Vis Sci 50(1):452–461
30. Sato K, Ohno-Oishi M, Yoshida M, Sato T, Aizawa T, Sasaki Y et al (2023) The GPR84 molecule is a mediator of a subpopulation of retinal microglia that promote TNF/IL-1α expression via the rho-ROCK pathway after optic nerve injury. Glia 71(11):2609–2622
31. Holan V, Palacka K, Hermankova B (2021) Mesenchymal stem cell-based therapy for retinal degenerative diseases: experimental models and clinical trials. Cells 10(3):588
32. Reboussin É, Buffault J, Brignole-Baudouin F, Réaux-Le Goazigo A, Riancho L, Olmiere C et al (2022) Evaluation of neuroprotective and immunomodulatory properties of mesenchymal stem cells in an ex vivo retinal explant model. J Neuroinflamm 19(1):63
33. Li Y, Zhang Y, Qi S, Su G (2018) Retinal organotypic culture—a candidate for research on retinas. Tissue Cell 51:1–7
34. Schnichels S, Paquet-Durand F, Löscher M, Tsai T, Hurst J, Joachim SC et al (2021) Retina in a dish: cell cultures, retinal explants and animal models for common diseases of the retina. Prog Retin Eye Res 81:100880
35. Rettinger CL, Wang HC (2018) Current advancements in the development and characterization of full-thickness adult neuroretina organotypic culture systems. Cells Tissues Organs 206(3):119–132

36. Alarautalahti V, Ragauskas S, Hakkarainen JJ, Uusitalo-Järvinen H, Uusitalo H, Hyttinen J et al (2019) Viability of mouse retinal explant cultures assessed by preservation of functionality and morphology. Invest Ophthalmol Vis Sci 60(6):1914–1927
37. Bull ND, Johnson TV, Welsapar G, DeKorver NW, Tomarev SI, Martin KR (2011) Use of an adult rat retinal explant model for screening of potential retinal ganglion cell neuroprotective therapies. Invest Ophthalmol Vis Sci 52(6):3309–3320
38. Abbhi V, Piplani P (2020) Rho-kinase (ROCK) inhibitors—a neuroprotective therapeutic paradigm with a focus on ocular utility. CMC 27(14):2222–2256
39. Buffault J, Brignole-Baudouin F, Reboussin É, Kessal K, Labbé A, Mélik Parsadaniantz S et al (2022) The dual effect of Rho-kinase inhibition on trabecular meshwork cells cytoskeleton and extracellular matrix in an in vitro model of glaucoma. J Clin Med 11(4):1001
40. Rao PV, Pattabiraman PP, Kopczynski C (2017) Role of the Rho GTPase/Rho kinase signaling pathway in pathogenesis and treatment of glaucoma: bench to bedside research. Exp Eye Res 158:23–32
41. Goldhagen B, Proia AD, Epstein DL, Rao PV (2012) Elevated levels of RhoA in the optic nerve head of human eyes with glaucoma. J Glaucoma 21(8):530–538
42. Shaw PX, Sang A, Wang Y, Ho D, Douglas C, Dia L et al (2017) Topical administration of a Rock/Net inhibitor promotes retinal ganglion cell survival and axon regeneration after optic nerve injury. Exp Eye Res 158:33–42
43. Murali A, Ramlogan-Steel CA, Andrzejewski S, Steel JC, Layton CJ (2019) Retinal explant culture: a platform to investigate human neuro-retina. Clin Exp Ophthalmol 47(2):274–285
44. Vohra R, Tsai JC, Kolko M (2013) The role of inflammation in the pathogenesis of glaucoma. Surv Ophthalmol 58(4):311–320
45. Hirata A, Inatani M, Inomata Y, Yonemura N, Kawaji T, Honjo M et al (2008) Y-27632, a Rho-associated protein kinase inhibitor, attenuates neuronal cell death after transient retinal ischemia. Graefes Arch Clin Exp Ophthalmol 246(1):51–59
46. Honjo M, Tanihara H, Inatani M, Kido N, Sawamura T, Yue BY et al (2001) Effects of rho-associated protein kinase inhibitor Y-27632 on intraocular pressure and outflow facility. Invest Ophthalmol Vis Sci 42(1):137–144
47. Nishio M, Fukunaga T, Sugimoto M, Ikesugi K, Sumi K, Hidaka H et al (2009) The effect of the H-1152P, a potent Rho-associated coiled coil-formed protein kinase inhibitor, in rabbit normal and ocular hypertensive eyes. Curr Eye Res 34(4):282–286
48. Zhou EH, Paolucci M, Dryja TP, Manley T, Xiang C, Rice DS et al (2017) A compact whole-eye perfusion system to evaluate pharmacologic responses of outflow facility. Invest Ophthalmol Vis Sci 58(7):2991–3003
49. Gao C, Huang L, Long Y, Zheng J, Yang J, Pu S et al (2013) Y-39983, a selective Rho-kinase inhibitor, attenuates experimental autoimmune encephalomyelitis via inhibition of demyelination. NeuroImmunoModulation 20(6):334–340
50. Nakagawa O, Fujisawa K, Ishizaki T, Saito Y, Nakao K, Narumiya S (1996) ROCK-I and ROCK-II, two isoforms of Rho-associated coiled-coil forming protein serine/threonine kinase in mice. FEBS Lett 392(2):189–193
51. Tanihara H, Inatani M, Honjo M, Tokushige H, Azuma J, Araie M (2008) Intraocular pressure-lowering effects and safety of topical administration of a selective ROCK inhibitor, SNJ-1656, in healthy volunteers. Arch Ophthalmol 126(3):309–315
52. Tokushige H, Inatani M, Nemoto S, Sakaki H, Katayama K, Uehata M et al (2007) Effects of topical administration of y-39983, a selective rho-associated protein kinase inhibitor, on ocular tissues in rabbits and monkeys. Invest Ophthalmol Vis Sci 48(7):3216–3222
53. Sagawa H, Terasaki H, Nakamura M, Ichikawa M, Yata T, Tokita Y et al (2007) A novel ROCK inhibitor, Y-39983, promotes regeneration of crushed axons of retinal ganglion cells into the optic nerve of adult cats. Exp Neurol 205(1):230–240
54. Yang Z, Wang J, Liu X, Cheng Y, Deng L, Zhong Y (2013) Y-39983 downregulates RhoA/Rho-associated kinase expression during its promotion of axonal regeneration. Oncol Rep 29(3):1140–1146
55. Tokushige H, Waki M, Takayama Y, Tanihara H (2011) Effects of Y-39983, a selective Rho-associated protein kinase inhibitor, on blood flow in optic nerve head in rabbits and axonal regeneration of retinal ganglion cells in rats. Curr Eye Res 36(10):964–970
56. Lingor P, Tönges L, Pieper N, Bermel C, Barski E, Planchamp V et al (2008) ROCK inhibition and CNTF interact on intrinsic signalling pathways and differentially regulate survival and regeneration in retinal ganglion cells. Brain 131(Pt 1):250–263
57. Bermel C, Tönges L, Planchamp V, Gillardon F, Weishaupt JH, Dietz GPH et al (2009) Combined inhibition of Cdk5 and ROCK additively increase cell survival, but not the regenerative response in regenerating retinal ganglion cells. Mol Cell Neurosci 42(4):427–437
58. Lambuk L, Mohd Lazaldin MA, Ahmad S, Iezhitsa I, Agarwal R, Uskoković V et al (2022) Brain-derived neurotrophic factor-mediated neuroprotection in glaucoma: a review of current state of the art. Front Pharmacol 13:875662
59. Lin S, Gao W, Zhu C, Lou Q, Ye C, Ren Y et al (2022) Efficiently suppress of ferroptosis using deferoxamine nanoparticles as a new method for retinal ganglion cell protection after traumatic optic neuropathy. Biomater Adv 138:212936
60. Huang Y, Peng J, Liang Q (2023) Identification of key ferroptosis genes in diabetic retinopathy based on bioinformatics analysis. PLoS ONE 18(1):e0280548
61. Li Z, Dong X, Wang Z, Liu W, Deng N, Ding Y et al (2005) Regulation of PTEN by Rho small GTPases. Nat Cell Biol 7(4):399–404
62. Semenova MM, Mäki-Hokkonen AMJ, Cao J, Komarovski V, Forsberg KM, Koistinaho M et al (2007) Rho mediates calcium-dependent activation of p38alpha and subsequent excitotoxic cell death. Nat Neurosci 10(4):436–443
63. Cherry JD, Olschowka JA, O'Banion MK (2014) Neuroinflammation and M2 microglia: the good, the bad, and the inflamed. J Neuroinflamm 11:98
64. Zhou T, Huang Z, Sun X, Zhu X, Zhou L, Li M et al (2017) Microglia polarization with M1/M2 phenotype changes in rd1 mouse model of retinal degeneration. Front Neuroanat 11:77
65. Roser AE, Tönges L, Lingor P (2017) Modulation of microglial activity by Rho-kinase (ROCK) inhibition as therapeutic strategy in Parkinson's disease and amyotrophic lateral sclerosis. Front Aging Neurosci 9:94
66. Ma H, Wang C, Liang S, Yu X, Yuan Y, Lv Z et al (2023) ROCK inhibition enhanced hepatocyte liver engraftment by retaining membrane CD59 and attenuating complement activation. Mol Ther 31(6):1846–1856
67. Ren L, Danias J (2010) A role for complement in glaucoma? Adv Exp Med Biol 703:95–104
68. Coyle S, Khan MN, Chemaly M, Callaghan B, Doyle C, Willoughby CE et al (2021) Targeting the NLRP3 inflammasome in glaucoma. Biomolecules 11(8):1239
69. Kanno S, Hirano S, Chiba S, Takeshita H, Nagai T, Takada M et al (2015) The role of Rho-kinases in IL-1β release through phagocytosis of fibrous particles in human monocytes. Arch Toxicol 89(1):73–85
70. Chen H, Deng Y, Gan X, Li Y, Huang W, Lu L et al (2020) NLRP12 collaborates with NLRP3 and NLRC4 to promote pyroptosis inducing ganglion cell death of acute glaucoma. Mol Neurodegener 15(1):26
71. Luo C, Yang X, Kain AD, Powell DW, Kuehn MH, Tezel G (2010) Glaucomatous tissue stress and the regulation of immune response through glial Toll-like receptor signaling. Invest Ophthalmol Vis Sci 51(11):5697–5707
72. Fletcher EL, Wang AY, Jobling AI, Rutar MV, Greferath U, Gu B et al (2019) Targeting P2X7 receptors as a means for treating retinal disease. Drug Discov Today 24(8):1598–1605
73. Déchelle-Marquet PA, Guillonneau X, Sennlaub F, Delarasse C (2023) P2X7-dependent immune pathways in retinal diseases. Neuropharmacology 223:109332
74. Di Virgilio F (2007) Liaisons dangereuses: P2X7 and the inflammasome. Trends Pharmacol Sci 28(9):465–472
75. Niyadurupola N, Sidaway P, Ma N, Rhodes JD, Broadway DC, Sanderson J (2013) P2X7 receptor activation mediates retinal ganglion cell death in a human retina model of ischemic neurodegeneration. Invest Ophthalmol Vis Sci 54(3):2163–2170
76. Yuan L, Neufeld AH (2001) Activated microglia in the human glaucomatous optic nerve head. J Neurosci Res 64(5):523–532

Publisher's Note